Geoderma 440 (2023) 116717

Contents lists available at ScienceDirect

Geoderma

journal homepage: www.elsevier.com/locate/geoderma

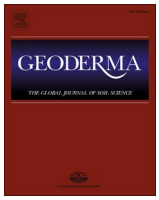

Accumulation of century-old biochar contributes to carbon storage and stabilization in the subsoil

Julien Fouché [a,*], Victor Burgeon [b], Jeroen Meersmans [b], Jens Leifeld [c], Jean-Thomas Cornelis [d]

[a] LISAH, Univ Montpellier, INRAE, IRD, Institut Agro, AgroParisTech, Montpellier, France
[b] TERRA Teaching and Research Centre, Gembloux Agro-Bio Tech, University of Liège, Gembloux 5030, Belgium
[c] Climate and Agriculture Group, Agroscope, Reckenholzstrasse 191, 8046 Zurich, Switzerland
[d] Faculty of Land and Food Systems, The University of British Columbia, Vancouver, BC, V6T 1Z4, Canada

ARTICLE INFO

Handling Editor: Cornelia Rumpel

Keywords:
Particulate organic matter
Mineral-associated organic matter
Dissolved organic carbon
Differential scanning calorimetry
PARAFAC modeling

ABSTRACT

Soil organic carbon (C) is a key component of the global C budget. As soil organic C turnover rates decrease with depth, agricultural practices favoring deep organic C storage will gain importance as long-term climate change mitigation strategies. In addition, amendment of pyrogenic organic matter (biochar) is considered a promising practice for sequestering C in croplands. However, so far the >30 cm depth soil organic C pool, and subsoil biochar dynamics in particular, has been understudied.

To address this, we focused on leftovers from pre-industrial charcoal kilns as a proxy to study the accrual of century-old biochar in the subsoil (30–100 cm) in comparison to adjacent control soil. Using thermal and elemental analyses as well as size and density fractionations (i.e., separating particulate and mineral-associated organic matter), we determined the distribution of pyrogenic organic C within the soil profile and investigated its stabilization in depth. We measured the dissolved organic carbon (DOC) concentrations as well as absorbance and fluorescence properties of dissolved organic matter (DOM) at different depths to characterize the effects of century-old biochar accumulation on the current leaching of DOM.

Our results showed that the presence of century-old biochar resulted in an increase of 53.8 ± 25.1 t C ha^{-1} in 0–100 cm, and 12 % of the pyrogenic organic C was stored in 30–60 cm. No difference in C stocks was observed in 60–100 cm between kiln sites and reference soils. Most of the pyrogenic organic C has been translocated as particulate organic matter, either free or occluded, to subsoils. This led to a change in the dominant fraction of organic matter in the E horizon; in reference soils 64.7 % of the total C was associated with mineral phases as opposed to only 42.3 % in soils enriched with biochar. The thermal analysis of the mineral-associated organic matter revealed that pyrogenic organic C was associated with mineral phases. With depth, DOC concentrations decreased and the relative contribution of microbial byproducts to fluorescent DOM increased. The soils enriched with century-old biochar displayed lower DOC concentrations and more aromatic DOM in the Ap horizon, which suggests biochar dissolution is still an on-going process. Our results suggest that the vertical transfers of century-old biochar mainly occurred as particle leaching in macroporosity and bioturbation but continuous dissolution has also contributed in these fine-textured cropland soils. In conclusion, the association of pyrogenic organic C with mineral phases as well as its migration in subsoil horizons promoted its physical disconnection from abiotic and biotic degrading agents, which likely contribute to the long-term stability of biochar.

1. Introduction

Soils, in particular in croplands, are increasingly considered as key players for climate change mitigation and adaptation (IPCC et al., 2019; Paustian et al., 2016). Globally, more than half of the soil organic matter (OM) stock is located in subsoil horizons (i.e., deeper than 30 cm) (Balesdent et al., 2018; Jobbágy and Jackson, 2000; Luo et al., 2019). A wide range of management practices aiming to sequester carbon (C) in soils (i.e., net transfer of CO_2 from the atmosphere into the soil for a given duration) through C storage (i.e., increase in organic C stocks over time in the soils of a given land unit) exist but differ according to the mechanisms targeted (Derrien et al., 2023). Some strategies increase C inputs to the soil while others reduce the accessibility of OM to decomposers. As organic C residence time increases with depth, strategies

* Corresponding author.

https://doi.org/10.1016/j.geoderma.2023.116717
Received 12 January 2023; Received in revised form 2 November 2023; Accepted 13 November 2023
Available online 25 November 2023

favoring subsoil organic C storage arouse interest in a long-term (i.e., centennial and longer) climate change mitigation perspective (Button et al., 2022). However, the efficiency assessment of sequestration practices relies on accurate understanding of mobility and persistence of OM in soils (Chenu et al., 2019).

The amendment of pyrogenic OM (i.e., biochar) stands among the most promising climate-smart approaches for its combined short-term and long-term C storage potential, long persistence in soils and agricultural benefits (IPCC et al., 2019; Joseph et al., 2021; Lehmann, 2007a; Smith, 2016). Biochar could be defined either as tailored solid organic material produced by heating biomass above 350 °C under controlled pyrolysis conditions with limited or no oxidant concentrations to prevent combustion without specific purpose (IPCC et al., 2019) or as pyrogenic OM specifically produced for amending soils (Bird et al., 2015). For the present study, we will use the terminology biochar for solid pyrogenic OM material, even if its amendment for agricultural purposes was not meant at the time of the pyrolysis.

Multiple *meta*-analyses have reported that biochar addition improved soil functions by increasing aggregate stability, porosity, pH and water holding capacity (Joseph et al., 2021). They have also shown that plant productivity increased due to an increase in nutrient supply and uptake by plants, a liming effect, favorable conditions for root growth and microbial activity and an overall increased resilience to disease and environmental stressors (Biederman and Harpole, 2013; Jeffery et al., 2011; Joseph et al., 2021). The greatest yield increases have been observed in low-nutrient acidic soils and sandy soils in the tropics and drylands (Crane-Droesch et al., 2013; Joseph et al., 2021). Biochar effects and properties evolve with time from quick dissolution (less than a month), reactive surface development (1–6 months) and aging (>6 months) (Joseph et al., 2021). Beyond improved soil functions and agronomic benefits, biochar addition has significant potential for C storage and sequestration (IPCC et al., 2019; Paustian et al., 2016). Pyrogenic OM displays long-term (centennial or longer) persistence in soil due to its recalcitrance against biotic and abiotic oxidation (Forbes et al., 2006), which is attributed to the high degree of aromaticity and condensation (Kuzyakov et al., 2014; Lutfalla et al., 2017; Wiedemeier et al., 2015). Although pyrogenic OM persistence in soils depends strongly on ecosystem properties (Schmidt et al., 2011) and organic precursor (Czimczik and Masiello, 2007), its recalcitrance increases with greater degree of aromaticity and condensation (Kuzyakov et al., 2014). During its stay in soils, biochar properties evolve over time through breakdown and surface oxidation (Cheng et al., 2006; Cheng and Lehmann, 2009; Brieuc Hardy et al., 2017). Several studies in field conditions investigated biochar effects during multiple seasons and years (Biederman and Harpole, 2013; Crane-Droesch et al., 2013; Jeffery et al., 2011; Joseph et al., 2021), but most of the studies investigating the effects of biochar aging and conducted in-situ are limited to <10 years (Joseph et al., 2021). Only few models exist to investigate centennial or longer aging of pyrogenic OM such as Amazonian Terra Preta soils, wildfire affected soils, industrial sites, relic kiln sites (Bird et al., 2015; Schmidt and Noack, 2000). The past production conditions and the precursor biomass differed strongly from current controlled settings of biochar production, which likely leads to different final pyrogenic materials (Bird et al., 2015). However, studies investigating biochar property changes at multi-year and centennial scales corroborate (Joseph et al., 2021). First, with time biochar undergoes physical breakdown of its structure, which creates fragments at the microscale and the nanoscale and further promotes dissolution (Spokas et al., 2014). Then, surface oxidation leads to the development of functional groups (i.e., carboxyl, phenol, carbonyl) (Cheng et al., 2008, 2006), the precipitation of phyllosilicates and carbonates onto biochar surfaces and the increase in total N content, H:C and O:C ratios (Hardy et al., 2017). These changes lead to greater cation exchange capacity, total N and available K+ concentrations, and promote organo-mineral associations such as aggregates and adsorption (Burgeon et al., 2022, 2021). In southern Belgium, pre-industrial charcoal production kiln sites have left biochar particles, which have been incorporated in cropland soils since their conversion from woodlands around 150–200 years ago (Hardy et al., 2017). The pyrolysis process in kiln sites, intended at producing charcoal as fuel for the steel industry, resulted in a product analogous to today's biochar produced from hardwood feedstocks at ~450 °C (Hirsch et al., 2017). Therefore these sites are an excellent model to unravel the long-term fate of biochar within soil profile. These pre-industrial kiln sites have been used previously to study biochar aging processes in the soil (Borchard et al., 2014; Burgeon et al., 2021; Hardy et al., 2017a; Hardy et al., 2017b; Mastrolonardo et al., 2019).

In addition to to be ubiquist and persistent in global topsoils (Reisser et al., 2016), pyrogenic OM is also prone to vertical transport (Bonhage et al., 2022; Hobley, 2019; Schiedung et al., 2020). This migration downwards enhances its disconnection with biotic and abiotic oxidation agents and its stability (Button et al., 2022). However, knowledge gaps remain regarding the long-term effects of biochar surface addition on its dissolution, vertical translocation and stabilization below 30 cm deep. The long-term fate of biochar in subsoil horizons is still poorly understood and quantified (Abiven et al., 2011; Button et al., 2022; Hockaday et al., 2007; Schiedung et al., 2020; Spokas et al., 2014). Before enabling widespread biochar adoption, studies investigating long-term biochar persistence and mobility in the 0–100 cm soil profile are required.

The potential mechanisms involved in translocating and stabilizing organic C in subsoils are dissolved organic carbon (DOC) leaching, living root rhizodeposition, root growth and decay, bioturbation and the physical translocation of particulate or mineral-bound OM as well as microbial activity and its necromass accrual (Button et al., 2022; Rumpel and Kögel-Knabner, 2011). Hence, the rate of vertical C migration depends on a combination of abiotic (e.g., water balance, infiltrability, texture) and biotic (soil fauna and vegetation) factors which vary significantly across ecosystems (Jobbágy and Jackson, 2000). As C migrates to the subsoil, its residence time tends to increase (Hicks Pries et al., 2023; Luo et al., 2019). Balesdent et al. (2018) showed that the majority of organic C present at 30 cm depth is characterized by a median age ranging between 100 and 300 years, whereas at 100 cm depth this corresponds to 1250 years. Luo et al. (2019) reported a large variation in subsoil organic C mean turnover times worldwide (i.e. ranging between 146 years for deserts and 3854 years for tundra). Organic C stability in subsoils (i.e., slower turnover) results from limited disturbance from cultivation (Button et al., 2022), lower relative abundance of both organic C and microbial biomass (Fontaine et al., 2007; Salomé et al., 2010), physical disconnection between decomposers and sources of OM (Dove et al., 2020; Heitkötter and Marschner, 2018; Salomé et al., 2010), and enhanced stabilization capacity because of the relatively higher content of reactive and unsaturated mineral surfaces and cations (Rasse et al., 2005; Rumpel and Kögel-Knabner, 2011), as well as dominance of oligotrophic conditions which limits microbial activity (Button et al., 2022; Dove et al., 2020; Salomé et al., 2010). However, fresh OM amendment can promote subsoil decomposition of millennia old OM through positive priming effects (Fontaine et al., 2007). While progressively incorporated deeper in the soil profile, OM is continuously processed resulting in a breaking down of OM into relatively smaller and oxidized biopolymers which coincides with the formation of microbial-derived compounds (Kaiser and Kalbitz, 2012; Roth et al., 2019) and decreased C:N ratios with depth (Rumpel and Kögel-Knabner, 2011).

Soil OM is composed of a continuum of various compounds, which differ in nature, recalcitrance (i.e., resistance to decomposition in given pedoclimatic conditions) and originate from both plants and microorganisms (Angst et al., 2021; Derrien et al., 2023). Multiple methods allow for characterizing the lability of soil OM to microbial processing and its persistence in soils (Derrien et al., 2023). Among them, protocols separating the bulk soil OM into fractions differing in size and density suitably characterize pools of contrasting composition, interactions with minerals and mean residence times (Lavallee et al., 2020; Poeplau et al., 2018). Physical fractionation protocols, generally using density and size thresholds respectively of 1.4–1.8 g cm^{-3} and size 50 μm, isolate two

main fractions: particulate organic matter (POM) and mineral-associated organic matter (MAOM) (Derrien et al., 2023; Lavallee et al., 2020). The POM refers to the mineral-free light fraction. It mostly originates from plant and fungi hyphae, and it is composed of a relative enrichment of structural organic compounds and displays high C/N ratios. While being preferentially used by soil microorganisms (mean residence time from shorter than 10 years to decades), POM is physically transferred into the soil and could persist due to its biochemical recalcitrance (e.g., pyrogenic OM), physical protection into aggregates and microbial inhibition due to edaphic conditions (e.g., low temperature, water logging) (Derrien et al., 2023; Lavallee et al., 2020). The MAOM typically refers to the heavier and finer fraction. It is defined as the fraction associated with silt- and clay-size minerals (Lavallee et al., 2020) and it is made of microbial necromass and byproducts as well as some plant compounds (Angst et al., 2021; Whalen et al., 2022). MAOM is enriched in nitrogen (N), displaying low C/N ratios, and persists in the soil thanks to chemical bonding to minerals (varying in nature and strength) and physical protection in aggregates. The C stabilized in the MAOM fraction can display mean residence time from decades to centuries and even millennials (Georgiou et al., 2022). Eusterhues et al. (2007) showed that MAOM could be ~2000 years older than the rest of the soil OM because old C is recycled in the microbial biomass (Derrien et al., 2023) and because bonding to minerals and occlusion decrease OM capacity to be metabolized (Fontaine et al., 2007; Lavallee et al., 2020). Some studies stressed the importance of differentiating OM in different particle size fractions (Kögel-Knabner et al., 2008; von Lützow et al., 2007) and POM occluded in aggregates of different sizes (Virto et al., 2010) for reaching functional OM fractions. Biochar amendment has been shown to increase POM content and C in the coarse sand, fine sand and silt and clay aggregate fractions after multiple years (Cooper et al., 2020). In similar soils from pre-industrial kiln sites, biochar enrichment promoted macroaggregation and pyrogenic OM was recovered both in free POM and associated with minerals occluded in aggregates and sorbed onto silt and clay sized minerals (Burgeon et al., 2021; Kerré et al., 2016).

Numerous analytical methods exist to identify, characterize and quantify pyrogenic OM, which are based either on physical separation, chemical oxidation, thermal analysis, spectroscopy and molecular marker analyses (Bird et al., 2015). These methods provide different results and these differences vary with the chemical composition and aging of pyrogenic OM (Bird et al., 2015; Kerré et al., 2016). Among them, thermal analysis and in particular differential scanning calorimetry (DSC) has been reported to be an efficient way to characterize the whole OM continuum and the different pyrogenic organic compounds by analyzing different proxies such as the heat flow at a given temperature, specific temperature at exotherm peaks, 50 % burn-off temperatures and by differentiating thermally labile and stable forms (Leifeld, 2007; Plante et al., 2009). In addition, experiments using standard additions of biochar to mineral soils free of pyrogenic OM and comparing with other analytical methods showed that DSC is suitable for quantifying biochar in bulk soils (Hardy et al., 2017; Kerré et al., 2016) and allows for quantifying pyrogenic organic C in size and density fractions (Burgeon et al., 2021). Although DSC relatively quantifies pyrogenic OM compared to control soils, its accuracy in similar kiln sites has been validated (Hardy et al., 2017; Kerré et al., 2016). The quantification of aged biochar has been shown to be challenging as its chemical and physical properties strongly evolve with continuous breakdown and surface oxidation (Hardy and Dufey, 2017; Kerré et al., 2016). Depending on the oxidation procedure, such as 'Walkley-Black' dichromate oxidation (Walkley and Black, 1934) or the chemo-thermal oxidation, the recovery of aged pyrogenic C contents differs (Kerré et al., 2016). Hardy and Dufey (2017) showed that the recovery of pyrogenic organic C by the dichromate oxidation is incomplete, and oxidation yield decreases with aging. DSC provides thermograms that allow for quantifying aged pyrogenic OM even for small samples such as fractions recovered from size and density fractionation.

In this study, our objective is to quantify the long-term (c. 200 years) effect of biochar surface accumulation on C storage in the subsoil and investigate the mechanisms involved. Numerous studies focused on artificially aged charcoal, however, to study processes involved in long term in-situ vertical migration, proxies from sites characterized by historical pyrogenic OM accumulation are needed (Bonhage et al., 2022; Hobley, 2019; Knicker, 2011). Here, we take the opportunity of the presence of century-old biochar (CoBC), derived from pre-industrial charcoal kiln sites, incorporated in soils. We compared 5 soils enriched in CoBC, visible as 20 m wide black spots on bare soils, to 5 adjacent reference soils, both modalities under conventional cropping in temperate climate.

In particular, we aim here to 1) quantify the long-term consequences of biochar accumulation on C stocks and stabilization in the 30–100 cm soil ayer, and 2) investigate the mechanisms involved in biochar vertical mobility. As aging leads to biochar structure physical breakdown promoting dissolution and therefore its potential for leaching (Spokas et al., 2014), we performed a size and density fractionation of soils and collected pore water for DOC analyses to investigate biochar physical breakdown, dissolution and further vertical mobility. In addition, aging and surface oxidation modify biochar thermal signature and interactions with minerals (Burgeon et al., 2021; Hardy et al., 2017; Brieuc Hardy et al., 2017; Leifeld, 2007), therefore we performed thermal analyses (i.e., DSC) to quantify and characterize pyrogenic OM in bulk soil and fractions characterized by different stabilization processes in the subsoil. We used a physical fractionation scheme previously applied in topsoils enriched with CoBC in the same site (Burgeon et al., 2021). The present study focuses on three main fractions differing in density and location in aggregates - the free light fraction (free LF), the occluded LF (occ. LF) and the heavy fraction (HF) - and shared in different aggregate-size classes - macroaggregates (250–2000 μm), microaggregates (50–250 μm) and silt and clay particles (<50 μm). To investigate vertical mobility of biochar through dissolution and leaching, we installed suction-cups and collected soil pore water at three different depths in CoBC and reference soils for six months. We analyzed each sample for dissolved organic carbon (DOC) and dissolved OM (DOM) optical properties using absorbance and fluorescence spectroscopy to characterize DOM aromaticity and investigate its origin. In addition, we performed PARAFAC modeling to identify the main components explaining the fluorescent DOM pool (Fouché et al., 2020). To our knowledge, the present study is the first to investigate the vertical mobility of biochar amendment over the long-term (c. 200 years) under temperate field conditions.

We hypothesize that historical surface accumulation of pyrogenic OM increased subsoil organic C stocks and pyrogenic C significantly contributes to this subsoil C storage. As century-old biochar accumulation led to an enrichment in pyrogenic OM as free and occluded POM in the topsoil horizon and assuming LF particle leaching being the main transfer process, we hypothesize that pyrogenic organic C occurred mainly as POM in the subsoils. We also hypothesize that century-old pyrogenic OM would be adsorbed to HF in the subsoil horizons thanks to dissolution and adsorption processes favored by breakdown and surface oxidation. Finally, we hypothesize that DOM from soils enriched in century-old biochar still display specific optical properties and contrasted DOC concentrations compared to reference soils.

2. Materials and methods

2.1. Study site

This study focuses on a Luvisol from the Belgian loam belt located in Isnes (Wallonia). In this region, fields are spotted with dark soil patches which occurred as a legacy from pre-industrial charcoal production in hearth mounds (Hardy et al., 2017). The selected study site, a 13 ha plot, was chosen as it contains multiple relic charcoal hearths and its representativeness of the conventional agriculture in the Belgian loam belt. The average annual precipitation on the site is of 840 mm of rain and the

mean annual temperature is 9.8 °C. The studied field undergoes a conventional rotation of four crops established since 1985, which alternates chicory (*Chichorium intybus L.*), winter wheat (*Triticum aestivum L.*), beet root (*Beta vulgaris L.*) and cover crops (a mixture of mustard and phacelia). Crops are regularly amended with mineral fertilizers and pesticides. Soil samples were collected after the destruction of the cover crops and before the chicory sowing in 2018. Soil water was collected with suction cups during the winter wheat growing season from February to August 2019.

In this site, 5 dark hearth patches were selected and studied as proxies for soils that have been enriched with century-old pyrogenic organic C (here called century-old biochar, CoBC). Adjacent to these patches (~40 m away), soils were studied as biochar free reference (REF). 2 modalities were therefore investigated in our work, CoBC and REF. The entire field displays a soil characterized as a Haplic Luvisol, dominated by a silt loam texture and developed on decarbonated loess (IUSS Working Group WRB, 2015). Three soil horizons were identified during a soil pit analysis, i.e. the C rich and plowed topsoil with ~15 % of clays, ~77 % of silts and 8 % of sands, referred to as the Ap horizon (0–30 cm), followed by a subsoil eluvial E horizon with ~18 % of clays, ~75 % of silts and 7 % of sands (30–60 cm) and a clay enriched Bt horizon with ~23 % of clays, ~72 % of silts and 5 % of sands (60–100 cm) (**Fig. S1**). No variation in soil horizon depth and thickness was observed within the field when each site was cored for soil sampling and pore-water suction cup installation. Therefore, all analyses and stock calculations were performed for 30 cm thickness in Ap and E horizons and 40 cm thickness for the Bt horizon. Baseline soil characteristics are available in Burgeon et al. (2022). The analysis and ancient soil maps (Ferraris, 1777 – Vandermaelen, 1846–1854 – "Cartes du dépôts de la guerre", 1865–1880) revealed that the study site was converted from forest to cropland *circa* 175–243 years ago. During this conversion, the soil plowing incorporated the biochar leftovers from hearths in the soil thus enabling us to claim the studied CoBC were roughly 200 years old.

2.2. Soil sampling and analysis

For CoBC and REF, samples were collected from 5 different locations in the studied field. Each sample was pooled as a composite from 3 soil cores to avoid punctual heterogeneities for each soil horizon (Ap, E and Bt). In the lab, samples were dried at 40 °C for 48 h, gently ground, sieved using a 2 mm grid prior to storage and further analyses.

The bulk densities (BD) of each soil type (CoBC and REF) and soil horizons (Ap, E and Bt) were determined in 3 soil pits. In each soil pit, two samples were collected per soil horizon using 100 cm^3 metal rings. The soil BD were calculated as the ratio of soil dry weight (60 °C – 48 h) to the known volume of soil. As all soils did not contain coarse elements (>2 mm), the soil BD corresponds to fine earth BD.

2.3. Soil fractionation

The full extent of the fractionation protocol set up in the present study is given in Burgeon et al. (2021), in which the topsoil horizon samples were fractionated, and described in detail in the supplementary information. Here, we performed the same fractionation protocol for samples of the 30–60 cm E horizon. The Bt horizon was not fractionated. For each modality, bulk soil samples from the 5 replicates followed a four-step fractionation protocol based on size and density (**Fig. S2**).

Step 1 – We followed a series of wet sieving to divide the soil into three aggregate size classes. We deposited 80 g of soil (previously submerged in distilled water for 5 min) on a 2 mm grid sieve sitting in a bath with 2 cm of distilled water covering the mesh (Cooper et al., 2020; Six et al., 1998). We simultaneously rotated and tilted the sieve for 50 rotations during 2 min. Subsequently, this sieve was back washed in a glass container and dried until complete evaporation (60 °C) whereas the finer material was deposited on a sieve 250 μm mesh. Next, the same approach was applied considering a sieve with a 50 μm mesh. Three fractions were obtained as an outcome to this fractionation procedure, i.e. the *coarse sand size* fraction (2000–250 μm), the *fine sand size* fraction (250–50 μm) and the *silt and clay size (S&C)* fraction (<50 μm). Any material coarser than 2000 μm, mostly composed of annual plant residues and with no visible century-old biochar particle, was discarded.

Step 2 – This step differentiated soil fractions based on their density using sodium polytungstate (SPT – 1.85 g cm^{-3}). We submerged 10 g of each of the three fractions of different size collected in step 1 in 50 mL of SPT. These were then gently shaken head over head 10 times to soak the sample and remove air bubbles and placed in a vacuum chamber (140 kPa) for 10 min then left to rest under atmospheric pressure for 20 min. All samples were then centrifuged at 4700 g for 10 min. The supernatant, considered as the light fraction (LF), was collected on glass fiber filters (0.45 μm). These operations were repeated thrice. Subsequently, the filters containing the free LF were thoroughly rinsed with distilled water and dried at 60 °C. Following the third centrifugation the pellet was shaken into suspension using distilled water in order to remove the SPT from the mineral dominated heavy fraction (HF). We then centrifuged (4700 g, 10 min) the suspension and discarded the distilled water. This cleaning operation was repeated thrice. From this procedure we obtained for both modality (CoBC and REF) and their 5 repetitions: *free LF* and *HF* of either *coarse sand*, *fine sand* or *S&C* size.

Step 3 – The *coarse sand size HF (*i.e.*, macroaggregates)* isolated from step 2 was placed on a 250 μm sieve installed on a shake plate and in a water bath with distilled water running through the sieve. The sample was in contact with 50 glass beads, shaked during 5 min, which led to aggregate breakdown. From this step, we isolated the *macroaggregate protected (Mp) fine sands* (>50 μm) and the *Mp-S&C* size fractions.

Step 4 – This final step was conducted in 4 phases. The first was a density fractionation using SPT to recover the *Mp-LF* from *Mp-S&C size HF*. The second phase broke down finer aggregates using ultrasonication set at 440 J mL^{-1} for 2 min (Soniprep 150 MSE) to free the *occluded LF* in macroaggregates, microaggregates and the S&C fraction. After ultrasonication of fractions we applied density fractionation using SPT in which we isolated *occluded LF* and *HF protected in macroaggregates*, *protected in microaggregates* or in *free S&C fractions*. Finally, wet sieving allowed for separating *mp-fine sand* and *mp-S&C particles*. From the step 4, we isolated the following fractions: *non-occluded Mp-LF, occluded Mp-LF, Mp-S&C size HF, occluded mp-LF, mp-fin sands, mp-S&C size HF, occluded LF and free S&C size HF*.

Following the soil fractionation, the bulk soil, the free LF and HF isolated during step 2 as well as the occluded LF and HF of step 4 (**Fig. S2**) were analyzed for C and N concentrations and thermal analysis. The C and N concentrations were determined via dry combustions using a Euro EA elemental analyzer (Hekatech, Germany). Prior to analysis, inorganic C was removed from mineral dominated HF samples through an acidification with HCl. Because insufficient material was obtained from the fractionation of the soil to enable an elemental analysis of free LF and occluded LF we pooled the replicates of each modality into a single sample.

Finally, we calculated the mass and C recovery for each fractionation step as the ratio between soil mass or C content gathered at the output of the fractionation step to that used as input for the same step. The weight recovery following the wet sieving (step 1) procedure was of 100.1 ± 0.2 % and 99.8 ± 0.3 % for CoBC and REF. For this same step, the C recovery was of 99.9 ± 13.8 % and 96.6 ± 24.6 % for CoBC and REF respectively. The weight recovery following step 4 was of 92.2 ± 1.6 % and 91.5 ± 0.6 % for CoBC and REF respectively. Finally, the C recovery for this step was of 80.9 ± 12.8 % for CoBC and 84.6 ± 13.8 % for REF.

2.4. Thermal analysis

We used differential scanning calorimetry (DSC) to analyze the thermal stability of OM and differentiate pyrogenic from non-pyrogenic forms. We used this method as previous studies showed that the quantification of pyrogenic organic C via DSC was correlated to oxidation

methods (Kerré et al., 2016) and molecular markers (Hardy et al., 2022), and because DSC could be performed on small soil fractions. Soil fractions were analyzed using simultaneous thermal analysis (Netzsch STA 449, Selb, Germany) from the Agroscope facilities in Zurich, Switzerland. Prior to analyzing our samples, the calorimeter was calibrated for temperature and sensitivity using six different known standards: indium, tin, bismuth, zinc, aluminum and silver.

3 bulk samples out of the 5 replicates were analyzed for each soil horizon (Ap, E and Bt) and for both CoBC and REF modalities. The 3 replicates (per modality) displaying the most similar soil C contents were selected for DSC analysis. We analyzed the free LF and HF isolated in step 2 as well as the occluded LF and HF obtained as outputs from step 4 of the fractionation procedure (highlighted in **Fig. S2**). As insufficient free LF and occluded LF were obtained to enable repetitions of the DSC analysis, we pooled the replicates of these different fractions into single samples for each modality. As such, for CoBC and REF soils, the occluded LF and the free LF were analyzed with no repetitions whereas HF were analyzed in triplicates. Prior to analysis, these samples were ground to powder. Roughly 20 mg were weighed in open aluminum pans for mineral dominated fractions (i.e. bulk soil samples and HF). For C rich fractions (occluded LF and free LF) 2 mg of material were diluted 10 times in Al_2O_3. A heating range between 50 and 700 °C was set for the analyses and heated at a rate of 20 °C min^{-1}. A synthetic air flow of 50 mL min^{-1} was set. To account for an increase in heat capacity of the sample, a baseline correction was drawn between 170 and 550 °C on the signal acquired. These two temperatures were selected as the offset of an endotherm caused by residual water contained in minerals on one hand and on the other as the onset of the quartz endotherm. To characterize the DSC curves, we used the peak heat flow (W g^{-1}), the C normalized heat flow (W gC^{-1}) and the corresponding signal temperature. The 50 % burnoff temperatures, (i.e. the temperature at which 50 % of the integrated heat has been evolved) was analyzed to compare samples. The soil C contents of all available bulk soil samples strongly correlated with the sum of peak heat flows per sample ($R^2 = 0.85$, p-value < 0.001).

We differentiated the thermally labile and thermally stable forms of organic C using a threshold temperature of 390 °C in which organic C is considered thermally labile below this threshold and thermally stable above this threshold. This cut-off temperature was chosen based on previous studies (Burgeon et al., 2021; Dell'Abate et al., 2000; Lopez-Capel et al., 2005). For soils in the CoBC modality, the pyrogenic OM was quantified as the additional heat flow occurring in the thermally stable part of the thermogram in CoBC soils compared to the heat flow in the stable region in REF soils. The sum of peak heat flows (i.e., peak heights) below 390 °C divided by the sum of peak heat flows corresponded to thermally labile C part of a sample. Similarly, the ratio of the sum of peak heat flows occurring above 390 °C to the sum of peak heat flows refers to the part of stable C of a sample. The labile or stable C content of a sample was calculated as the product of these ratios and the C content of the sample. Finally, the pyrogenic organic C content of a fraction of CoBC is calculated as follows (the remaining C content is considered as non pyrogenic organic C) on thermograms normalized by the sample C content:

$$PyOC = \frac{CoBC_{stable} - REF_{stable}}{CoBC_{total}} * CoBC_C \quad (1)$$

***Equation (1)** – Quantification of pyrogenic organic C content (PyOC, g 100 g^{-1}) in soil samples (fractions or bulk soils). CoBC and REF, the two concerned modalities. Stable, the C normalized peak heat flow occurring above 390 °C. Total, the sum of C normalized peak heat flows characterizing a sample in CoBC samples. $CoBC_C$: the C content of the studied sample.*

The quantification of the pyrogenic C content is based on the assumption that REF soils do not contain pyrogenic OM. However, the historical plowing of the field has likely led to incorporate some pyrogenic OM from the kiln sites into current REF soils. Therefore the calculated pyrogenic C content could be considered as an excess compared to reference soils, thus likely being underestimated.

2.5. Soil solution sampling and analyses

To study the solubility of century-old biochar in soils we collected soil pore water in CoBC and REF modalities from February to August 2019 during winter wheat growing season. Borosilicate suction cups (1 μm mesh) were inserted at a 20° angle with respect to a vertical axis in the three soil horizons (i.e. 20, 45 and 80 cm) for the 5 field replicates of each studied soil for a total of 45 suction cups. Each suction cup was connected to a 1 L vacuum resistant glass bottle in which a depression ranging between 140 and 600 hPa was applied. This suction was fixed based on two tensiometer readings as measured in the E horizon. When the soil became too dry for sampling the pumping was halted, limiting sampling periods to cold and rainy seasons. Soil pore water samples were stored in fully filled pre-combusted (550 °C) and acidified amber glass vials. After field sampling, all waters were refrigerated at 4 °C. DOC analyses were conducted on 44 CoBC and 37 REF pore water samples within 2 months following sampling and optical properties of DOM were analyzed within 9 months. We acknowledge that losses of DOC and related decreases in DOC concentrations could occur while kept refrigerated and in the dark prior to being analyzed (Nachimuthu et al., 2020). However, as both REF and CoBC water samples were collected at the same time and kept at 4 °C for the same period, we assume that possible DOC decline did not alter the observed concentration differences. In addition, for a specific site and depth, no systematic decrease with time within the two months of maximum conservation period was observed.

DOC concentrations were measured by applying high-temperature combustion by making use of a TOC Analyzer (LOTIX Combustion, Teledyne Tekmar, Mason, OH, USA). Milli-Q blanks and standards were run prior to and following every 5 samples. A new calibration was generated for each DOC run of at most 20 samples. Concentrations of DOC were calculated as the mean of three injections with a coefficient of variance <5 % (detection limit = 0.3 mg/L, analytical uncertainties = 3.6 %).

Optical properties of DOM were investigated to explore their origin in the soil. UV–visible absorbance and fluorescence measurements and Emission Excitation Matrices (EEM) were performed at room temperature (Horiba-Jobin spectrometer Yvone Scientific Edison, NJ) using the Horiba EzSpec v1.2.0.32 software (BGeoSys, ULB, Belgium). Each sample was analyzed individually in 1 cm pathlength quartz cuvette. Absorbance spectra were blank-corrected using Milli-Q water. UV–visible absorbance spectra and excitation values were collected between 255 and 600 nm at 3 nm step increments and emission wavelengths were scanned from 280 to 600 nm. Band pass for excitation and emission was 5 nm and integration time was 0.2 s. We used the EzSpec software correction procedure to correct EEMs files for blanks and inner filter effects, and removed 1st and 2nd order Rayleigh scatter. The signal was normalized to Raman Units by dividing EEM intensities by the integral of the Raman peak of MilliQ samples which was located at an excitation of 350 nm at emission ranging between 371 and 428 nm (Lawaetz and Stedmon, 2009).

Six different indices were determined based on absorbance and fluorescence measurements to characterize the DOM, i.e. the specific UV absorbance (SUVA254, L mgC^{-1} m^{-1}), the total fluorescence (Raman Unit), the total fluorescence normalized by DOC concentration (RU L mgC^{-1}), the fluorescence index (FI), and the humification index (HIX). Furthermore, we decomposed the 111 collected EEMs into individual fluorescent compounds (fluorophores) by running a parallel factor analysis (PARAFAC).

$SUVA_{254}$ was calculated as the decadal UV absorbance at 254 nm divided by the DOC concentration. $SUVA_{254}$ is positively correlated to bulk DOM aromaticity (Weishaar et al., 2003) therefore dissolved PyOC would display higher $SUVA_{254}$ values (Tang et al., 2016). The total fluorescence was calculated as the sum of EEMs and further normalized by the DOC concentration to determine the difference in contribution of the fluorescent dissolved organic matter (FDOM) to the entire DOM pool. FI was calculated as the ratio of emissions between 450 and 500

nm at an excitation wavelength of 370 nm (McKnight et al., 2001). It illustrated the source of DOM from plant and soil organic matter derived (~1.2) to microbial products (~1.8) (Fellman et al., 2010). HIX was calculated as the area under the emission spectra between 435 and 480 nm divided by the peak area over two spectral bands 300–345 nm + 435–480 nm, at an excitation of 254 nm (Fellman et al., 2010). HIX increase illustrated a shift of emission maximum towards longer wavelengths related to a greater abundance of high-molecular weight aromatic fluorescing molecules with lower H:C ratios (Birdwell and Engel, 2010; Fellman et al., 2010).

PARAFAC models decomposed fluorescence data that are arranged in three-dimensional arrays (i.e. sample × excitation wavelength × emission wavelength) into accurate spectra and relative concentrations (in Raman Unit) of known fluorescent groups showing similar chemical composition in a complex DOM mixture (Murphy et al., 2008, 2013). PARAFAC individual compounds refer to compound groups such as humic-like, fulvic-like or protein-like with distinct optical properties rather than single organic compounds (Fellman et al., 2010). PARAFAC modeling was performed using the staRdom package v1.0.18 (Pucher et al., 2019) in R software v4.2.2 (R Core Team, 2022) in order to separate EEMs into independent fluorescent compounds. Excitation and emission wavelengths below 270 nm were removed from matrices to avoid deteriorating signal-to-noise ratios. Prior to modeling, regions of the spectra influenced by 1st and 2nd order scatter peaks were omitted. A five-compound model was generated incorporating a total of 102 samples of which 9 samples were considered as outliers and removed from the model. Model parameters were constrained to be non-negative. The model, which identified compounds with unimodal emission maxima, was validated using residual analysis, split-half analysis and random initialization (Murphy et al., 2013; Pucher et al., 2019; Stedmon and Bro, 2008) and explained 99.8 % of the total fluorescence signature. For each sample, the intensity of each PARAFAC compound was normalized to the total fluorescence and expressed as the relative contribution of each compound to the total fluorescence. The identified compound emission and excitation spectra were compared with previous studies investigating biochar DOM optical properties and using the open fluorescence database (Murphy et al., 2014) (https://openfluor.lablicate.com/). The 5 compounds have been previously reported by studies available in the openfluor database (Tucker Congruence Coefficient, TCC > 0.95) and in studies in cropland soil with recent biochar amendments (Table 1). The description and likely structures of these 5 compounds based on their excitation and emission wavelengths are reported in Table 1.

2.6. Data analysis

We pursued the comparison of soil C, N and C:N ratios of bulk soil using a one factor analysis of variance (ANOVA) and classified means using a least significant differences test (LSD test) to differentiate modalities and horizons (p value < 0.05). Similarly, the analysis of soil fractions compared masses, C and N contents and concentrations as well as C:N ratios for a given fraction (step 2 free LF, step 2 HF, step 4 occ. LF

Table 1
Description and likely structure of the five fluorescent compounds characterized by the PARAFAC modeling and determined based on EEMs in comparison to previous studies and Openfluor database comparison.

Component	Excitation max (nm)	Emission max (nm)	Description and likely structure	Source of DOM	Fellman et al., 2010 Review	Liu et al., 2019 Soils & Biochar	Eykelbosch et al., 2015 Soils & Biochar	Jamieson et al., 2014 Biochar	Openfluor comparisonb (component with TCC > 0.95)
1	<270	435	UVA Humic-like or fulvic like fluorophores, similar to peak A in Cobble 1996	Terrestrial	C6	–	A	C2	27
2	<270	380	UVA humic-like – Low molecular weight aromatic fluorophores associated with microbial activity. Optical properties close to syringaldehyde (producted in breakdown of lignin). Similar to peak C in Cobble 1996	Terrestrial, Autochtonous, Marine	C4	–	–	C1	22
3	360–365 (<270)	450	UVC humic-like - High molecular weight, aromatic and condensed fluorophores, abundant in wetlands	Terrestrial	C10	–	–	–	16
4	<270	490–510	UVA humic-like or fulvic like - High molecular weight, syringaldehyd-like (byproducts of lignin breakdown), associated with high DOM contents, soil-derived DOM, ubiquituous in freshwater environment	Terrestrial	C5	C2	–	C4	33
5	340	410	Humic-like, associated with microbial activity with antrhopogenic origin found in agriculturally dominated watersheds	Terrestrial, Autochtonous, Marine	C15	C1	C	–	3

*number of studies reporting similar emission and excitation wavelenghts found in the openfluor database.

and step 4 HF). Per fraction we compared size classes and soil types (CoBC and REF). For each fraction we differentiated means using a one-way ANOVA and classified means based on a LSD test ($p < 0.05$).

For the analysis of DSC results, signal treatments and presentation were undertaken using R v.4.4.2 (R Core Team, 2022). Bulk soil samples and HF are represented as the mean ± sd of triplicates whereas only one replicate exists for free or occluded LF. Similarly, to the elemental composition analysis, the comparison of indicators was pursued by a one-way ANOVA and the classifications of means pursued through a LSD test. Only DSC peak heights on soil HF were compared by pairs based on site location between CoBC and adjacent REF soil using a student paired *t*-test. The threshold p-val remained of 0.05 for all tests. A Wilcoxon rank sums test was used on soil pore water samples to compare their DOC contents, and indices characterizing DOM optical properties by pairs according to combinations of given horizons (Ap, E and Bt) and modality (CoBC, REF).

To ensure a trustworthy fractionation protocol the mass recovery was determined as the sum of fractions weight for a given step divided by the sample weight used as input to this fractionation step. We calculated the weight recovery for steps 2 and 4. Similarly, we calculated the C content recovery as the sum of C content per fractionation step over the C content of the fraction used as input material.

3. Results

3.1. Total C and N distribution in the soil profile

In the 0–30 cm Ap horizon, BD was lower in CoBC than REF soils (Table 2). BD increased with depth and was similar in E and Bt horizons in modalities. The organic C contents decreased with depth from 26.4 ± 5.1 to 3.6 ± 1.0 g kg^{-1} in CoBC and from 13.8 ± 0.4 to 3.2 ± 1.0 g kg^{-1} in REF (Table 2). The organic C content was 1.8 times higher in the E horizon in CoBC (8.0 ± 2.8 g kg^{-1}) than in REF soils (4.4 ± 2.0 g kg^{-1}) but similar in the Bt horizon of the two modality. CoBC soils had 64.2 ± 25.7 % higher N content than REF soils in the Ap horizon, but no significant difference in horizons E and Bt (Table 2). C:N atomic ratios decreased with depth from 13.2 ± 1.7 to 7.5 ± 1.9 in CoBC and from 11.5 ± 0.6 to 6.6 ± 1.5 in REF (Table 2). While atomic C:N ratios tend to be higher in all horizons in CoBC compared to REF soils, differences were not significant.

In the Ap horizon (0–30 cm), organic C stocks were 93.5 ± 18.1 tC ha^{-1} in CoBC and 54.6 ± 1.6 tC ha^{-1} in REF soils, representing 71 % higher stocks in CoBC (Table 2). In the E horizon (30–60 cm), C stocks were 35.5 ± 12.3 tC ha^{-1} in CoBC and 20.0 ± 8.9 tC ha^{-1} in REF soils, which represents 78 % higher stocks in CoBC than in REF soils (Table 2). Overall, the subsoils horizons (E and Bt) represented 37.8 ± 9.2 % and 40.9 ± 6.2 % of the 0–100 cm organic C stocks in CoBC and REF soils, respectively. For the 0–100 cm thickness, summing the three horizons (Table 2), soils in the CoBC modality stored 150.4 ± 22.8 tC ha^{-1} (from 123.7 to 189.4 tC ha^{-1} among replicates) as opposed to between 93.8 ± 12.1 tC ha^{-1} in REF soils (from 81.8 to 115.9 tC ha^{-1}). This represented an average increase of ~60 % in C stocks for the 0–100 cm thickness in CoBC compared to REF soils.

3.2. Aggregation patterns and elemental analysis of 30–60 cm layer fractions

The mass distribution between fractions following the soil fractionation revealed no differences in terms of aggregation patterns between CoBC and REF in the E horizon (30–60 cm, Table 3). Following the wet sieving and the density fractionation (end of step 2), the weight of the coarse sand size fraction was equal to that of the fine sand size fraction and heavier than the silt and clay fraction for both CoBC and REF soils (Table 3). The weights of free LF were similar between CoBC and REF in the different size classes even though coarse sand size free LF dominated free LF fractions (Table 3). Free LF as coarse sand size particles contributed to 53 % and 41 % of the free LF in CoBC and REF soils, respectively (Table 3). Similarly, results produced by the last fractionation step (4) showed no significant differences in the weight of the occluded-LF between studied modalities (Table 3).

The relative contribution of the different fractions (all size classes combined for free LF from step 2, occluded LF and HF from step 4) to the total soil C content is illustrated in Fig. 1 as a function of depth (the topsoil data originates from Burgeon et al., 2021). The C distribution among fractions showed the HF (step 4) contribution to soil organic C content increased with depth for both REF and CoBC soils, and its contribution in the E horizon was higher in REF than in CoBC soils (CoBC = 42 ± 11; REF = 65 ± 8 % of soil organic C, Fig. 1). The relative contribution of free LF to total soil C content increased with depth in CoBC but not in REF soils (Fig. 1). The increase in HF and free LF contributions was mostly at the expanse of occluded LF (step 4) in both modalities. In CoBC soils, free LF (step 2) represented 39 ± 10 % while occluded LF represented 19 ± 14 % of the C content of the E horizon. In the E horizon, the free LF of coarse sand size (step 2) displayed the greatest fraction C content (2.5 ± 1.3 g kg^{-1}) in CoBC soils, but not in REF soils (0.4 ± - g kg^{-1}, Table 3).

The elemental analysis of free LF and HF (step 2) showed no meaningful differences in N contents as a function of the size class (Table 3). However, when summing N contents in free LF (step 2) of different size classes according to modalities (CoBC & REF), the total N content of CoBC was higher than that in REF soils (CoBC = 0.12 ± 0.05; REF = 0.05 ± 0.02 g kg^{-1} - Table 3). Similarly, when summing the N contained in HF of different size classes (step 4 HF), more N was found in CoBC than in REF soils (CoBC = 0.82 ± 0.15; REF = 0.66 ± 0.16 g kg^{-1} - Table 3).

Results showed higher atomic C:N ratios in free LF than HF for both soil types and no significant differences as a function of size. Furthermore, when comparing HF isolated by step 2 (density fractionation) and step 4 (ultrasonication), C:N ratios of HF from step 4 (~4.3) were smaller than HF from step 2 (~6) for both modalities.

Table 2
Bulk density (BD), C, pyrogenic organic C (PyOC), N distributions in the bulk samples. Contents are expressed in g kg^{-1} soil, stocks in tC ha^{-1}. BD values were used to determine C stock of a given horizon. Results are expressed as mean ± sd. A letter indicates significant differences between modalities across horizons (LSD-test, p-val < 0.05). No PyOC is found in REF (-). No significant trace of PyOC can be distinguished in the DSC thermogram of CoBC Bt Horizon (ns).

	Depth cm	BD g cm^{-3}	C g kg^{-1}	N g kg^{-1}	C:N	C t ha^{-1}	PyOC g kg^{-1}	PyOC t ha^{-1}
CoBC	**Ap (0–30)**	1.18 ± 0.11 a	26.4 ± 5.1 a	2.3 ± 0.2 a	13.2 ± 1.7 a	93.5 ± 18.1 a	8.2 ± 3.4	30.5 ± 12.8
REF		1.32 ± 0.07b	13.8 ± 0.4b	1.4 ± 0.1b	11.5 ± 0.6 abc	54.6 ± 1.6b		
CoBC	**E (30–60)**	1.48 ± 0.05c	8.0 ± 2.8c	0.7 ± 0.2c	12.5 ± 1.1 abc	35.5 ± 12.3c	0.9 ± 0.4	4.2 ± 1.9
REF		1.51 ± 0.01c	4.4 ± 2 d	0.5 ± 0.1c	9.5 ± 2.8 bcd	20.0 ± 8.9 d		
CoBC	**Bt (60–100)**	1.49 ± 0.05c	3.6 ± 1 d	0.6 ± 0.1c	7.5 ± 1.9 d	21.5 ± 6.1 d	ns	ns
REF		1.50 ± 0.06c	3.2 ± 1 d	0.6 ± 0.1c	6.6 ± 1.5 cd	19.2 ± 5.9 d		

Table 3
Mass & elemental analyses of subsoil fractions (E horizon). C (%) and N (‰), the C and N concentrations of a fraction, C and N (g kg^{-1}) the content of C and N of a fraction for 1 kg of bulk soil (i.e., fraction C concentration multiplied by fraction mass). Results are presented for the two major fractionation steps: 2 & 4 and expressed as mean ± sd and a letter indicating significantly different values (LSD-test, p-val < 0.05) as a function of the size class and the modalities for a given fractionation step. p values are presented for differences at a given fractionation step. No values (-) are indicated when insufficient material was gathered during the fractionation to enable an elemental analysis or repetitions. Note the C concentration and content of occluded fractions are deduced as the difference between step 2 and step 4 HF.

		size (μm)	mass (g kg −1)		C (%)	C (g kg −1)		N (‰)	N (g kg −1)		C:N (-)
step 2 - free LF	**CoBC**	2000–250	4.1 ± 2.0	a	63.1 ± 3.2	2.6 ± 1.3	a	17.6 ± 6.8	0.07 ± 0.05		41.3 ± 20.9
		250–50	2.4 ± 1.2	ab	39.4 ± 4.1	0.9 ± 0.4	b	14.9 ± 6.5	0.04 ± 0.02		29.2 ± 9.8
		<50	1.2 ± 0.2	b	28.2 ± 11.7	0.3 ± 0.1	b	11.1 ± 1.7	0.01 ± 0.00		24.8 ± 7.2
	REF	2000–250	3.5 ± 0.0	a	10.6 ± -	0.4 ± -	b	5.8 ± 0.0	0.02 ± 0.00		18.2 ± -
		250–50	2.1 ± 0.0	ab	10.1 ± 1.6	0.2 ± 0.0	b	5.1 ± 2.6	0.01 ± 0.01		22.0 ± 8.2
		<50	3.0 ± 2.6	ab	8.6 ± 2.0	0.2 ± 0.2	b	5.5 ± 5.0	0.02 ± 0.02		27.5 ± 23.8
						p < 0.05					
step 2 - HF	**CoBC**	2000–250	392.7 ± 28.7	a	0.5 ± 0.3	2.0 ± 1.1	a	0.9 ± 0.4	0.34 ± 0.16	a	6.3 ± 2.1
		250–50	330.1 ± 53.5	ab	0.5 ± 0.2	1.6 ± 0.8	a	0.8 ± 0.2	0.26 ± 0.11	ab	6.0 ± 1.5
		<50	270.8 ± 40.0	bc	0.4 ± 0.2	1.1 ± 0.5	a	0.7 ± 0.3	0.19 ± 0.09	abc	6.1 ± 2.7
	REF	2000–250	410.0 ± 120.5	a	0.4 ± 0.1	1.5 ± 0.7	a	0.6 ± 0.3	0.27 ± 0.13	ab	6.6 ± 3.0
		250–50	364.1 ± 107.5	a	0.3 ± 0.1	0.9 ± 0.1	a	0.5 ± 0.2	0.19 ± 0.11	bc	5.9 ± 3.0
		<50	218.8 ± 59.3	c	0.2 ± 0.1	0.5 ± 0.2	b	0.5 ± 0.1	0.10 ± 0.01	c	4.8 ± 1.9
			p < 0.001			*p < 0.05*			*p < 0.05*		
step 4 - occ. LF	**CoBC**	2000–250	0.9 ± 0.5	a	73.0 ± -	0.7 ± -		–	–		–
		250–50	1.1 ± 0.5	ab	56.8 ± -	0.6 ± -		–	–		–
		<50	0.3 ± 0.0	ab	72.5 ± -	0.2 ± -		–	–		–
	REF	2000–250	1.4 ± 0.0	ab	19.8 ± -	0.3 ± -		–	–		–
		250–50	0.4 ± 0.0	b	0.8 ± -	0.0 ± -		–	–		–
		<50	0.7 ± 0.0	ab	–	–		–	–		–
			p < 0.05								
step 4 - HF	**CoBC**	2000–250	350.2 ± 31.5	a	0.4 ± 0.1	1.3 ± 0.4		1.1 ± 0.4	0.39 ± 0.13		3.5 ± 0.9
		250–50	298.0 ± 48.8	ab	0.3 ± 0.1	1.0 ± 0.4		0.8 ± 0.2	0.23 ± 0.06		4.3 ± 0.7
		<50	264.7 ± 39.1	ab	0.3 ± 0.1	0.8 ± 0.2		0.8 ± 0.1	0.21 ± 0.04		4.2 ± 1.2
	REF	2000–250	355.0 ± 111.6	a	0.3 ± 0.2	1.3 ± 0.8		0.8 ± 0.2	0.28 ± 0.11		4.6 ± 2.7
		250–50	336.2 ± 99.8	a	0.3 ± 0.1	0.9 ± 0.1		0.7 ± 0.2	0.24 ± 0.10		4.4 ± 2.0
		<50	215.0 ± 59.4	b	0.3 ± 0.1	0.6 ± 0.3		0.7 ± 0.3	0.15 ± 0.07		4.8 ± 2.2

3.3. *Thermal analysis and pyrogenic organic C distribution in the profile*

The use of DSC on bulk soil samples revealed the presence of pyrogenic OM in the Ap and E horizons but not in the Bt horizon, as shown by higher heat flows from CoBC than from REF, at temperatures above 390 °C (Fig. 2). In the Ap horizon the presence of pyrogenic organic C was marked by three additional heat flows occurring at 386 ± 3 °C, 435 ± 2 °C and 520 ± 1 °C in CoBC bulk samples but unseen in REF soils.

In the E horizon, the presence of biochar was marked by a higher heat flow occurring in CoBC soils (above 390 °C). The thermograms of bulk samples were characterized by a sharp exotherm occurring at CoBC = 318.3 ± 4.2 °C and REF = 322.3 ± 0.6 °C and a second smaller exotherm occurring at CoBC = 432.7 ± 6.7 °C and REF = 437.0 ± 5.2 °C (Fig. 2). This second exotherm peak also occurred in the Ap horizon. In the Bt horizon, no trace of pyrogenic organic C was detected for bulk samples as the first exotherm occurred for both modalities at 323.0 °C ± 0.3 and the shoulder at 439.0 ± 0.5 °C with similar stable:total ratios (Fig. 2). No significant difference in 50 % burnoff temperature occurred between modalities in the E horizon (CoBC = 324.2 ± 6.6; REF = 320.5 ± 2.8 °C) nor Bt horizon (CoBC = 321.8 ± 1.9; REF = 321.5 ± 2.7 °C) (**Table S1**).

An analysis of mineral associated OM (HF – step 4) in different horizons and according to size classes (Mp, mp, S&C) revealed the presence of pyrogenic organic C in all HF marked as an shoulder occurring at ~400 °C. This was particularly visible in the Ap horizon (**Fig. S3**). In the E horizon the presence of biochar was characterized by a shoulder in the thermogram occurring at ~400 °C (Fig. 3). Furthermore, in the E horizon, CoBC HF thermograms are characterized by an overall higher heat flow per unit C (values reported in Fig. 3) than in the Ap horizon (**Fig. S3**) with relatively larger increases in heat flow in CoBC than in REF soils. For both CoBC and REF, free or occluded LF thermograms showed that a majority of the heat flow occurred above 400 °C in both horizons (Fig. 3, **Table S1**). The single replicate available per size class (for occluded LF and free LF) suggested a decrease of heat flow per unit C occurring in the E horizon particularly so for macro (Mp) and micro-protected (mp) LF compared to fractions of the Ap horizon (Fig. 3, **Fig. S3**). Finally, free LF in the CoBC E horizon showed the same three visible exotherms as bulk samples (Fig. 2, Fig. 3) as well as for hand-picked PyOC (Burgeon et al., 2021), which revealed the presence of pyrogenic organic C in LF fractions. However, no difference in 50 % burn-off temperature of the HF fractions (step 2 and step 4) occurred between modalities in the E horizon (**Table S1**). The HF (step 4) in CoBC showed greater stable:total heat flow ratios than REF (**Table S1**). In the E horizon, the stable:total heat flow ratios of free LF and occluded LF of S&C size were slightly higher in CoBC than REF soils (**Table S1**). Therefore, using the same methodology as for bulk soil samples, ~25 % of the total pyrogenic organic C in the E horizon occurred as associated with mineral phases, showing a majority of pyrogenic organic C in the E horizon occurs as free or occluded LF (**Table S1**).

Along the 0–100 cm soil profile, the thermally stable:total peak ratio (i.e., similar to stable:total heat flow ratio) for bulk CoBC soils was significantly higher compared to bulk REF soils in the Ap (CoBC = 43 ± 2 %; REF = 19 ± 5 %) (Burgeon et al., 2021) and E horizon (CoBC = 28 ± 5 %; REF = 16 ± 2 %) but not different in horizon Bt (CoBC = 20 ± 1 %; REF = 20 ± 2 %, **Table S1**). Using stable:total peak ratios on bulk soil samples we quantified pyrogenic organic C contents of 0.9 ± 0.4 g kg^{-1} of soil and stocks of 4.2 ± 1.9 tC ha^{-1} in the 30–60 cm E horizon (Table 2). CoBC soils in the 0–100 cm stored 34.7 ± 12.9 t ha^{-1} of pyrogenic organic C and the 30–60 cm accounted for 12 ± 4 % of the total pyrogenic organic C in the 0–100 cm.

The Fig. 4 illustrates similar stocks in stable C for both modalities (stable:total) as well as an increase in total C caused by the presence of PyOC in CoBC soils. For both Ap and E horizons, additional labile OM is visible in CoBC soils. Indeed in the Ap horizon, CoBC soils had on average a greater stock of non-pyrogenic organic C of ~8.4 t ha^{-1} compared to REF soils, which represented 22 % of the C stock difference between modalities. In the E horizon, non-pyrogenic organic C contributed to ~11.3 t ha^{-1} (73 %) of the stock difference between CoBC

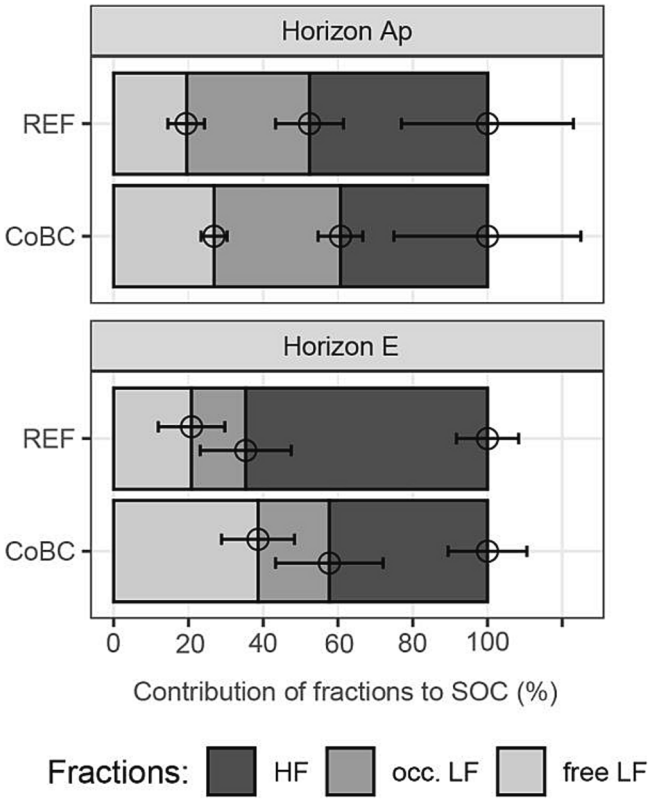

Fig. 1. Relative contribution of fractions to total soil C according to horizons in the Ap horizon (0–30 cm) and the E horizon (30–60 cm). C distributions are shown according to the studied modalities (CoBC & REF) and horizons for heavy fraction (HF), occluded light fractions (occ. LF) or free light fractions (free LF). Free LF originates from the step 2 while occluded LF and HF from the step 4 of the fractionation protocol. Data for the topsoil is available in Burgeon et al. (2021).

and REF and pyrogenic organic C accounted for between 5.7 % and 16.6 % of the total organic C content (Table 2).

3.4. DOM concentrations and optical properties

The DOC concentration of soil pore water decreased with depth and was significantly lower in CoBC compared to REF for the Ap and E horizons (Fig. 5). $SUVA_{254}$ values (i.e., increasing with bulk DOM aromaticity) decreased with depth and were higher in CoBC than REF for the Ap horizon (Fig. 5). FI (values close to 1.8 indicate mainly microbial derived fluorescent DOM (FDOM) and values close to 1.2 mainly plant derived FDOM) increased with depth but did not differ with REF (Fig. 5). HIX (higher values correspond to more aromatic and condensed FDOM) decreased with depth and did not show any differences among soil horizons (Fig. 5). The total fluorescence of DOM was slightly correlated with DOC concentrations ($R^2 = 0.26$, $p < 0.001$) and decreased with depth but did not differ between CoBC and REF for a given depth (**Fig. S4**). The fluorescence of DOM normalized by DOC concentration was strongly correlated with $SUVA_{254}$ ($R^2 = 0.95$, $p < 0.001$) (**Fig. S4**).

Five fluorescent compounds were identified through PARAFAC modeling on pore water samples of the studied modalities combined. Their relative contribution to FDOM as well as their respective EEM are presented in **Fig. S5**. Our results showed no differences in relative abundance between compounds C1, *C2* and C5 when comparing the two modalities (**Fig. S5**). Compound C1, which represents a group of high molecular weight and aromatic organic compounds, was the dominating (~45 % total fluorescence) fluorophore in the Ap horizon and its contribution to FDOM strongly decreased with depth (~35 % total

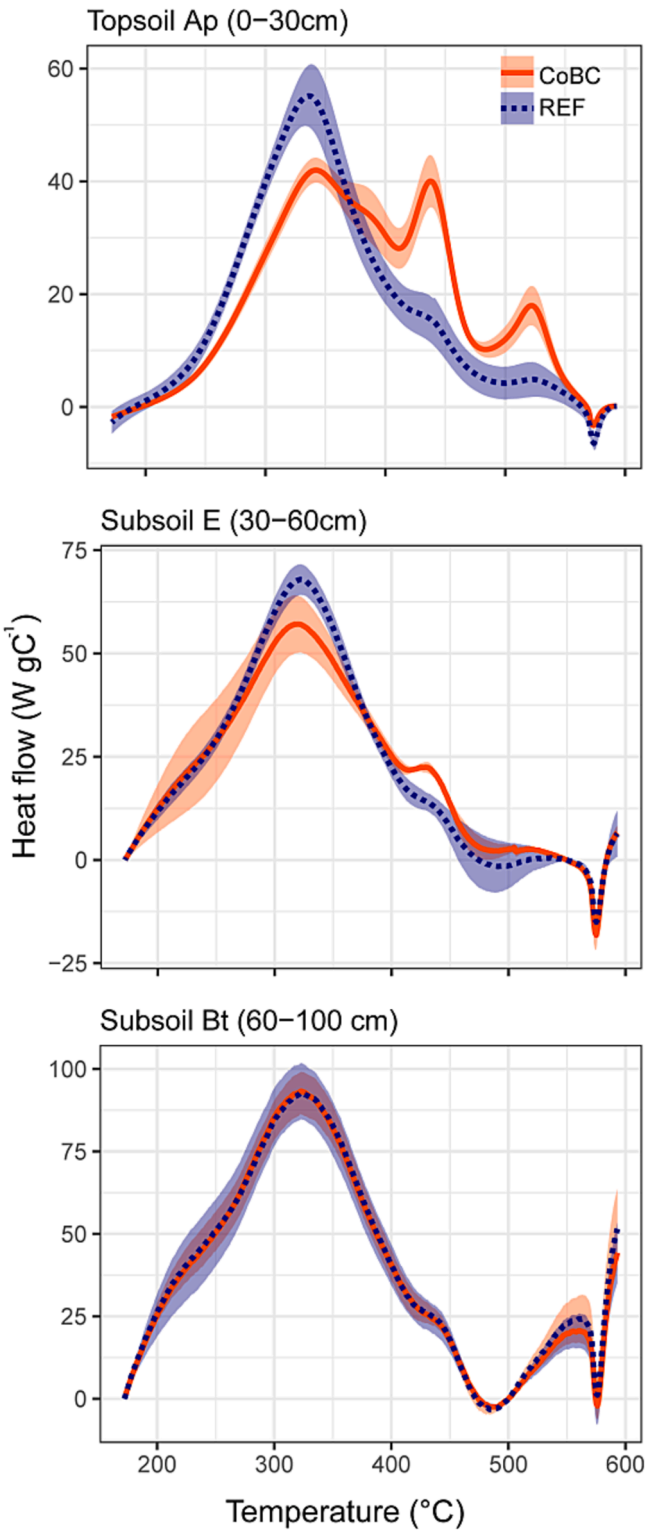

Fig. 2. Thermograms of bulk soil samples with or without pyrogenic organic C (CoBC and REF) as a function of depth. The heat flow is normalized by the organic C content of samples. Per given depth each line represents the mean ± sd, n = 3 independent field replicates.

fluorescence). Inversely, the contribution of compounds *C2* & C5, which both represented low molecular weight and microbial derived organic compounds increased with depth (**Fig. S5**). Compound C3, which represented high molecular weight, aromatic and condensed fluorophores, displayed a lower contribution in the Ap horizon of CoBC than in REF

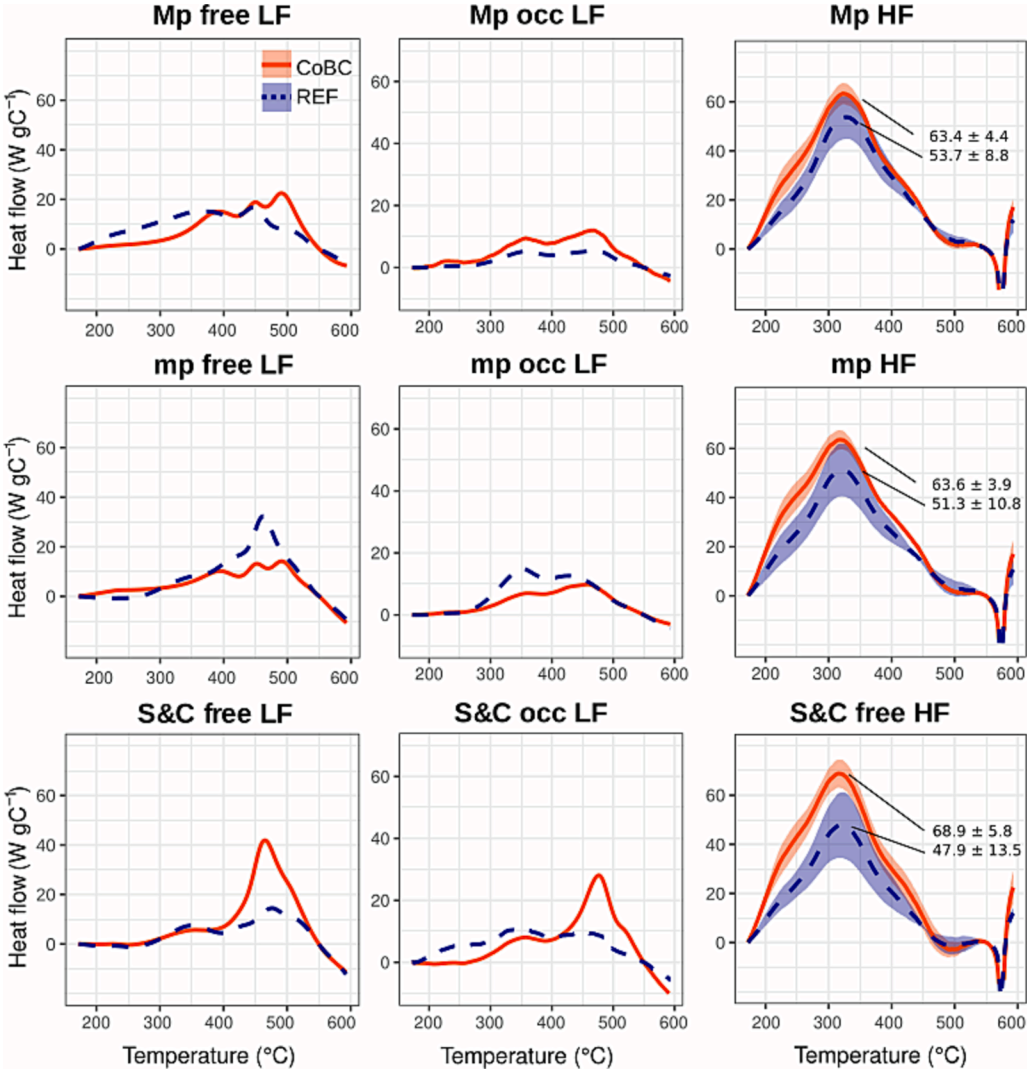

Fig. 3. Thermograms of the free light fraction (free LF, step 2), the occluded light fraction (occ LF, step 4) and the heavy fraction (HF, step 4) according to size classes (Mp: macroaggregate protected, mp: microaggregate protected or free) in the E horizon (30–60 cm). For free LF and occ LF, the replicates were combined to allow for DSC analysis. For HF, each line is the mean ± sd, n = 3 independent field replicates. Values report the mean maximum punctual heat flow ± sd for both studied modalities (W gC^{-1}).

soils. In the E horizon, C3 was relatively less abundant in CoBC than REF soils. Finally, compound C4, highly conjugated and associated with lignin breakdown, was similarly commonly found in REF and CoBC soils (**Fig. S5**).

4 Discussion

4.1. Effects of century-old biochar on C stocks in the topsoil and subsoil layers

To compare our results to international and national estimates of soil organic C stocks, we used the methodology developed by Meersmans et al. (2009) for Flanders (adapted based on the Belgian soil classification). For the studied Luvisol of the REF modality, soil C stocks were of 37 ± 3 tC ha^{-1} at 0–30 cm (Ap), 18 ± 1 tC ha^{-1} at 30–60 cm (E) and 13 ± 1 tC ha^{-1} at 60–100 cm (Bt) and 68 ± 3 tC ha^{-1} over 0–100 cm (Meersmans et al., 2009). These estimates are slightly lower than the C stocks calculated from our field measurements (Table 2). However, they are very similar to the global estimates for Luvisols (all land uses considered) of 31 tC ha^{-1} and 65 tC ha^{-1} for 0–30 cm and 0–100 cm respectively (Batjes, 1996). More precisely, for this particular region (i.e. the Belgian loess belt), cropland Luvisols have been reported to hold ~42 tC ha^{-1} in the plowing layer, showing that the C stock of our studied REF soil is slightly above average (Goidts and van Wesemael, 2007).

The variability of C stocks in-between replicates of REF and CoBC soils resulted from differences in the initial amount of biochar leftovers at hearth sites following charcoal production and the past land use. The western part of the field had been a grassland until more recently than the eastern part, which led to greater C contents in the north-west replicates. The century-old biochar accumulation led to an increase in organic C stocks of 53.8 ± 25.1 tC ha^{-1} compared to reference soils in the 0–100 cm profile (Table 2). Pyrogenic organic C represented 30.5 ± 12.8 tC ha^{-1} in CoBC of which 12.1 ± 7.5 % was found in the E horizon (Table 2). While CoBC soils stored 35.9 ± 18.8 tC ha^{-1} more C than REF in the 0–30 cm Ap horizon, representing a 68 % increase, the relative difference in C stocks between CoBC and REF soils was of 78 % in the 30–60 cm E horizon (Table 2). The surface accumulation of biochar led to the downward transfer of pyrogenic OM after ~200 years and to subsoil C storage. However its effects on the soil C dynamics have been limited to 60 cm deep as no difference in C stocks, pore-water DOC concentrations and DOM optical properties were observed deeper. The

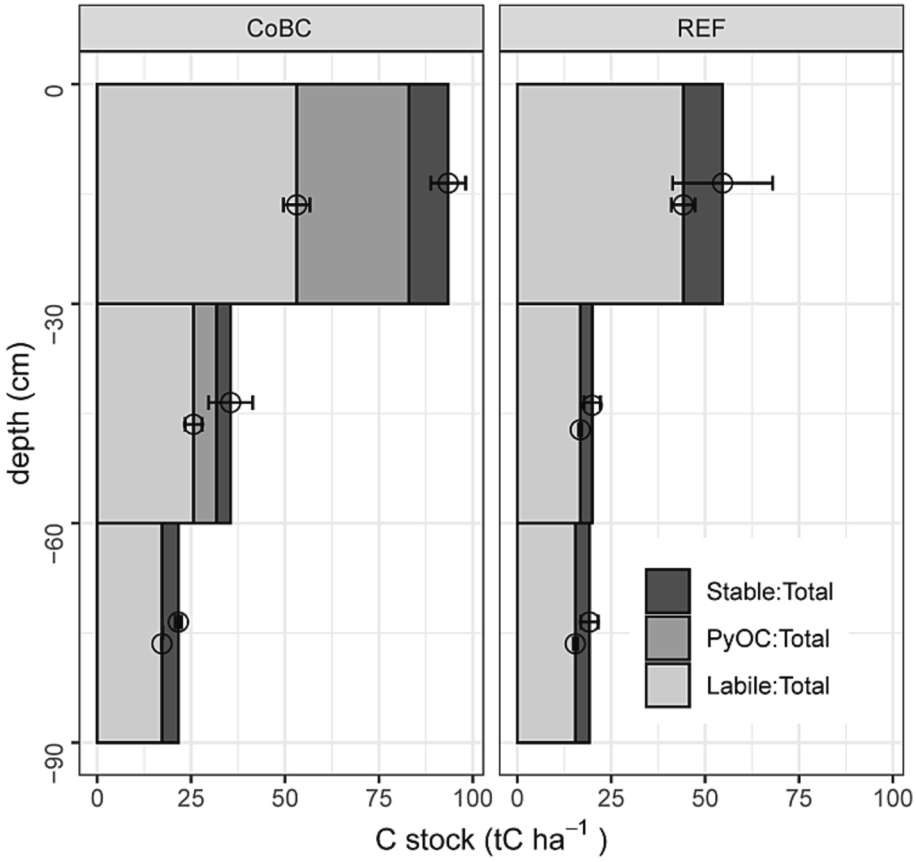

Fig. 4. Soil organic C and pyrogenic organic C (PyOC) distribution as a function of depth. The bar plot represents the evolution of C stocks (tC ha^{-1}) as a function of depth and per studied soil (CoBC & REF). The thermally stable or labile forms of organic C are represented in the bar plot and used to identify the amount of pyrogenic organic C in CoBC.

relatively low C contents of REF soils and the difference in organic C stocks between modalities brings forward the large potential for C storage of Luvisols, even deeper than 30 cm, through agricultural practices favoring OM inputs into soils (Chenu et al., 2019; Derrien et al., 2023; Stewart et al., 2007). Considering a C concentration ranging between 70 % and 90 % in pyrogenic OM on one hand (depending on pyrolysis conditions) and the mass yield of ~30 % (ratio between fresh feedstock and pyrogenic C mass) on the other (Jiang et al., 2017; Lehmann, 2007b), we estimated that approximately 130–170 t ha^{-1} of hardwood were needed to produce the 34.7 tC ha^{-1} of pyrogenic organic C reported here.

Given that the initial amount of biochar deposited on the kiln site and the mineralization rate of biochar are unknown (Bowring et al., 2022), determining a precise vertical transportation rate is complicated. However, when roughly 12 % of the actual total pyrogenic organic C stock occurs in the E horizon, and considering ~30 cm vertical migration (30–60 cm) over 200 years' residence time and neglecting mineralization losses, an indicative transport rate of 1.5 mm yr^{-1} can be estimated from this study. This is very close to the transport rate of 2.35 mm yr^{-1} after 200 years estimated by Rumpel et al (2015). Such a small vertical migration rate and limited fractions recovered below 30 cm, can be explained by the low water infiltrability of the fine textured soils and the potential for pyrogenic C retention onto mineral phases (Hobley, 2019; Major et al., 2010; Schiedung et al., 2020). Schiedung et al. (2020) showed in a column experiment that only a limited fraction of pyrogenic OM was vertically transferred and fine textured soils had the potential for absorbing mobilized pyrogenic OM. In addition, pyrogenic organic C retention was shown to increase with depth in particular fine textured soils (Schiedung et al., 2020). Therefore, we can assume that transport rates decrease with depth, explaining the absence of pyrogenic organic C below 60 cm.

DSC represents an operationally defined method for quantifying pyrogenic C in soil, which is based on the overall higher thermal stability of pyrogenic as compared to non-pyrogenic organic moieties. Using DSC enabled us to quantify pyrogenic organic C in small soil fractions separated by size and density and in soil layers depleted in organic C, which no other method could have performed. However, this procedure is not a direct quantification of pyrogenic organic C content. It consists in estimating the content of pyrogenic organic C by comparing ratios in peak height and differences in C content between modalities. Our quantification of the amount of pyrogenic carbon was based on the assumption that no pyrogenic OM is found in REF soils. However, it is likely that REF soils contained a small amount of pyrogenic OM as all soils do (Reisser et al., 2016; Soucémarianadin et al., 2019). The historical plowing of the field has likely led to adding some biochar particles from the kiln sites into areas outside of the dark patches. Therefore the presented estimates based on DSC could be considered as an excess in pyrogenic organic C compared to a reference, meaning the pyrogenic organic C stocks in CoBC are underestimated.

Hardy et al. (2017a), who used standard additions of biochar to mineral soils free of pyrogenic organic C, reported that pyrogenic organic C content in kiln site soils accounted for 79.5 % of the difference in C content between surface layers of CoBC and REF soils (Hardy et al., 2017). This linear relationship corresponds well with our estimates for the Ap horizon (Burgeon et al., 2021) but not for the E horizon where pyrogenic organic C represented ~27 % of the C content difference (Table 2). These differences in the contribution in pyrogenic organic C in CoBC compared to REF among horizons could result from different processes governing OM accrual in topsoil and subsoil layers (Button et al., 2022). First, OM accumulation can result from greater plant

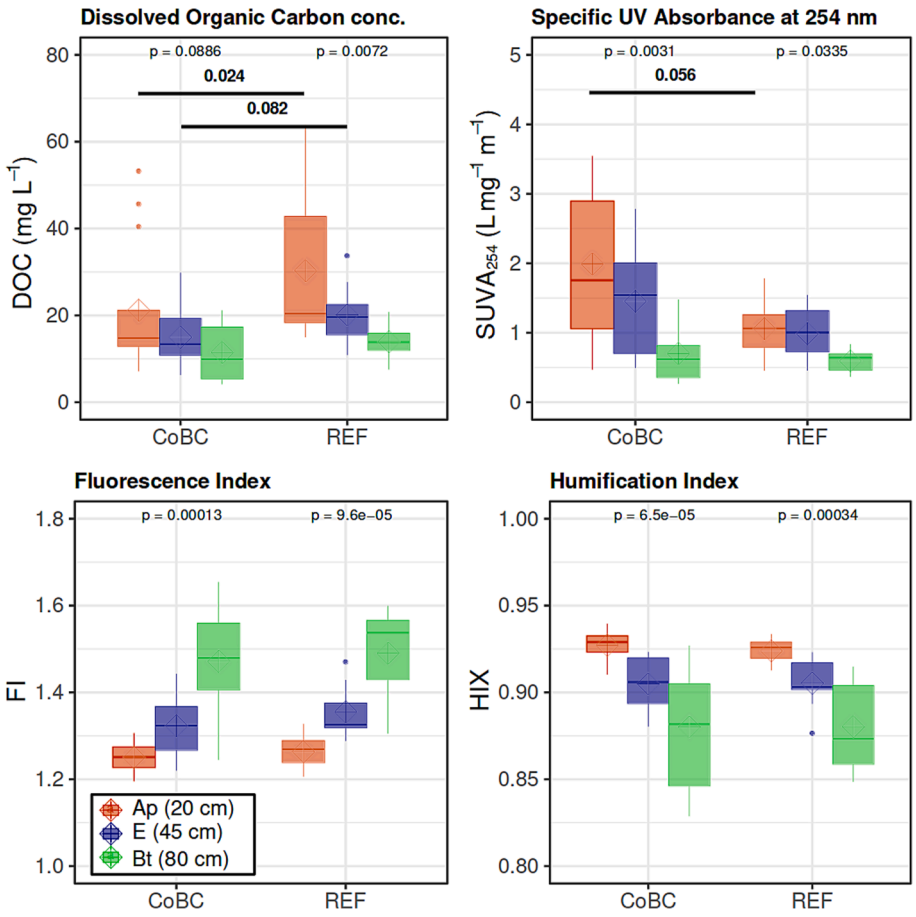

Fig. 5. Dissolved organic carbon concentration, Spectific UV Absorbance at 254 nm ($SUVA_{254}$), fluorescence index (FI) and humification index (HIX) for soil pore water samples collected in the two studied modalities (CoBC & REF) at 20 cm (in Ap horizon), 45 cm (in E horizon) and at 80 cm (in Bt horizon). The above p-values indicate the significance of the distribution difference among the horizons for each modality using Kruskal-Wallis test (i.e., smaller p values indicate greater significance of the median difference). Values in bold font indicate the significance of distribution difference between similar horizons of different modalities using paired Wilcoxon test.

productivity and higher aboveground and belowground OM inputs driven by biochar accumulation (Joseph et al., 2021). However, there is a global consensus that biochar-driven yield increases are limited in nutrient-rich loamy soils in temperate climate (Crane-Droesch et al., 2013; Joseph et al., 2021). More specifically, two studies conducted in the same field showed that the harvested crop yields of both winter wheat (Heidarian Dehkordi et al., 2020a) and chicory roots (Heidarian Dehkordi et al., 2020b) did not differ between CoBC and REF soils. Therefore, we can assume OM accrual in CoBC compared to REF soils, in particular in 30–60 cm depth, did not result from increased aboveground and belowground plant productivity. Then, biochar addition can lead to storage in non-pyrogenic OM due to modification in microbial carbon use efficiency, adsorption of root exudates, microbial metabolites and microbial necromass, and protection in aggregates with improved aggregation (Burgeon et al., 2021; Cooper et al., 2020; Hardy et al., 2017; Joseph et al., 2021). The greater non-pyrogenic OM increase in the E horizon compared to the Ap horizon could result from a higher proportion of microbial-derived proteins and root exudates in depth than in the topsoil, which have a strong potential for binding pyrogenic organic compounds (Brodowski et al., 2005; Kleber et al., 2007; Poirier et al., 2018). Our study shows that the addition of a relatively small amount of pyrogenic OM could contribute to store non-pyrogenic OM in soil horizons below 30 cm deep.

4.2. Surface pyrogenic organic C accumulation induced a shift from MAOM to POM as the main fraction in the 30–60 soil layer

The elemental analysis of soil fractions from the E horizon showed that in REF soils most of the C was associated with mineral phases in HF (REF = 64.7 ± 8.3 %; CoBC = 42.3 ± 10.6 % total organic C) whereas in CoBC soils, the majority of C was found as LF, POM either free or occluded within aggregates. The MAOM fraction accounted for comparable C stocks for both CoBC and REF soils in the E horizon (Table 3). Our values of C contents of the MAOM and its contributions to the total soil C pool fall in the reported values in croplands (Begill et al., 2023; Georgiou et al., 2022; Rocci et al., 2021). The MAOM fraction dominates the soil C stocks in cropland soils, which are relatively poor in OM, as the POM is quickly processed and poorly replenished as the plant biomass is massively exported (Cotrufo et al., 2019; Lugato et al., 2021). However, higher heat flow below 390 °C of the HF fractions in CoBC than REF soils (Fig. 3) suggest the presence of pyrogenic organic C led to a significant accrual of non-pyrogenic in the MAOM fraction.

The differences in C stocks between CoBC and REF modalities mainly resulted from the greater C contents of free or occluded POM (REF = 35.3 ± 8.3 %, CoBC = 57.5 ± 10.6 %). This result validated our hypothesis that century-old biochar accumulation led to an enrichment in pyrogenic OM as free and occluded POM in the subsoils. These results vouch for pyrogenic organic C migration downwards to the subsoil through bioturbation or physical transport of particles through porosity (Hobley, 2019). The vertical mobility of biochar as POM has previously

been reported (Bonhage et al., 2022; Major et al., 2010; Schiedung et al., 2020). For free POM to migrate downwards by leaching, their affinity to mineral phases must be relatively small to avoid being retained in the topsoil and their size should be small enough to be able to move within soil pores (Schiedung et al., 2020). Interestingly, particles of coarse sand size were the most abundant of the three free LF size classes for the topsoil (Burgeon et al., 2021) and the subsoil. This repartition suggests a preferential leaching of sand-size POM and may result from a limited affinity with mineral phases for big particles, whereas smaller ones tend to be occluded as observed in the Ap horizon (Burgeon et al., 2021). Inversely the bigger the particle the more it was expected to be retained mechanically from vertical movement. Therefore, the lower occurrence of pyrogenic POM as large sand size in the E horizon, as compared to the Ap horizon, may result from the limited migration rate. It could explain the relatively low amount of pyrogenic OM in depth below 30 cm and its absence below 60 cm. It suggests that leaching in macroporosity could be the main vertical transfer process. In these fine textured soils, the in-situ observations of multiple worm casts supported that bioturbation could also be a dominant mechanism involved in the vertical distribution of pyrogenic POM (Carcaillet, 2001; Eckmeier et al., 2007; Major et al., 2010).

The occluded LF was the smallest of the three C pools in the E horizon (REF = 14.5 ± 12.16 %, CoBC = 19.07 ± 14.4 %). Here, the mass recovery after soil fractionation did not allow for an elemental analysis of the occluded LF, therefore, the C contained in this fraction was estimated as the difference between the total C content and the sum of carbon contained in the free LF and HF, and considering the DOC fraction as negligible (~0.2 % of total soil organic C, data not shown). Nonetheless, our results suggested occluded LF were less prone to vertical migration in comparison to free POM and MAOM likely due to physical protection, which is favored by bioturbation (Vidal et al., 2019). For the Luvisol studied here, occlusion was particularly important for the topsoil Ap horizon (Burgeon et al., 2021). Differences in OM distribution among fractions raises the question of the role of aggregation in C stabilization and limiting vertical migration in subsoils.

4.3. *Biochar accumulation led to DOC adsorption and continuous pyrogenic organic C dissolution after ~200 years*

Regardless of larger soil organic C contents in CoBC soils, our results revealed lower concentrations of DOC in the soil pore water for the Ap horizon (0–30 cm) than in REF soils. These findings differ from results of previous field and batch experiments with addition of biochar, which showed higher DOC concentrations (Liu et al., 2019; Yang et al., 2022) or no significant differences (Major et al., 2010). The lower DOC contents reported here for CoBC could result from a higher sorption of non-pyrogenic DOM onto pyrogenic particles in the Ap horizon (Brodowski et al., 2005; Kerré et al., 2017; Smebye et al., 2016). While biochar aging through oxidation was shown to favor its solubility (Abiven et al., 2011), aging also improves retention of DOC by sorption with the appearance of functional groups onto pyrogenic particles (Cheng et al., 2006).

As expected, absorbance and fluorescence indices (e.g., $SUVA_{254}$, FI, HIX) showed that plant derived material (e.g., high $SUVA_{254}$, low FI) dominated the DOM in the Ap horizon while in the Bt horizon DOM was mainly derived from microbial compounds (e.g., decreasing $SUVA_{254}$, increasing FI with depth). As such, our results agreed with the commonly accepted paradigm whereby, plant-derived dissolved organic compounds are continuously processed, co-precipitated and sorbed along the soil profile leading to changes in aromaticity and molecular weight of DOM (Kaiser and Kalbitz, 2012; Roth et al., 2019). As a consequence, DOM and soil OM are both dominated by microbial by-products in subsoil horizons (Angst et al., 2021; Kaiser and Kalbitz, 2012; Roth et al., 2019; Rumpel and Kögel-Knabner, 2011).

The optical properties of DOM differed among soils only in the Ap horizon (0–30 cm). The bulk DOM displayed a greater aromaticity in CoBC than in REF soils (i.e., higher $SUVA_{254}$ values). Interestingly, no significant differences in fluorescence indices (i.e., FI, HIX, total fluorescence, fluorescence normalized by DOC concentration) were observed between modalities. The $SUVA_{254}$ index was the most suitable tool to trace the dissolution of century-old biochar. Dissolution of condensed structures through solubilization of pyrogenic organic C and increased solubilization with aging was observed by Abiven et al. (2011). However, in a field experiment, Liu et al. (2019) did not observe significant differences in $SUVA_{254}$ and fluorescence indices between control and biochar treatments. Our results clearly showed the continuous solubilization and leaching of aged pyrogenic organic C from surface layers ~200 years after biochar accumulation. We can assume that biochar aging, through the decrease in hydrophobicity and related increase in solubility (Aller et al., 2017), promoted its dissolution and leaching downwards. Our findings support previous studies which showed continuous export of black carbon from catchments affected by historical fires (Dittmar et al., 2012; Hockaday et al., 2007; Wagner et al., 2018). It highlights that surface pyrogenic organic C accrual could sustain its cycle from terrestrial to aquatic ecosystems over the long term.

The use of PARAFAC modeling enabled the identification of five major compounds used to characterize DOM and provided insights into the solubilization patterns of pyrogenic or non-pyrogenic OM. Compounds C1, C2 and C5 (Table 1) displayed similar contributions to the total FDOM between soils and appeared as commonly found compounds in agricultural settings (Fellman et al., 2010) regardless of the presence of biochar in the soil (Liu et al., 2019). Interestingly, compound C3, which is characterized by more aromatic compounds of high molecular weight, contributed the least to total fluorescence in Ap and E horizons in CoBC soils as compared to REF. This suggested that, in CoBC soils, aromatic high molecular weight non-pyrogenic OM compounds were sorbed and microbially processed in topsoil horizon and hence did not migrate vertically (Kaiser and Kalbitz, 2012; Roth et al., 2019). Abiven et al. (2011) showed based on a batch experiment testing the solubility of pyrogenic OM (chestnut, pyrolysis T = 450 °C), that 10-year-old charcoal released between 40 and 55 times more condensed structures than fresh charcoal, showing not only that biochar released very aromatic molecules but also that this is the consequence of aging. Optical properties showed that century-old biochar was likely solubilized into aromatic compounds (i.e., higher $SUVA_{254}$) but PARAFAC modeling did not provide a specific fluorophore related to pyrogenic organic C dissolution and migration to subsoils.

Overall our results on the dissolved fraction corroborates DSC analysis on POM and MAOM fractions. The DSC analysis of soil fractions showed that between 0.08 and 0.12 g of pyrogenic C for kg^{-1} of soil occurred as MAOM. This accounted for between ~25 % of the total pyrogenic organic C reported for the E horizon. The presence of dissolved century-old biochar and pyrogenic C onto MAOM fractions suggests that, beyond transport as particles, pyrogenic organic C could be continuously dissolved, leached and adsorbed onto minerals. Pyrogenic organic C dissolves in the topsoil, moves in subsoil as DOM and is finally adsorbed on reactive mineral surfaces where pyrogenic organic C retention increases, in particular in fine-textured soils (Abiven et al., 2011; Brodowski et al., 2005; Sokol et al., 2018, Schiedung et al., 2020).

5. Conclusions

Here, we performed elemental and thermal analyses on bulk samples and size and density fractions in the 30–60 layer in soils enriched in century-old biochar and their reference counterparts. We studied unique settings where biochar was produced in charcoal kilns approximately 200 years ago and incorporated in conventionally cropped fields since. We quantified the pyrogenic organic C contents and stocks in soils and fractions in three layers: 0–30, 30–60 and 60–100 cm.

The surface accumulation of biochar 200 years ago led to subsoil C storage as indicated by the 30–60 cm E horizon containing 78 % more C in CoBC than in REF soils. In 0–100 cm, the biochar addition resulted in

a additional stock of 53.8 ± 25.1 t C ha^{-1} of which 34.7 ± 12.9 t ha^{-1} was pyrogenic organic C. The 30–60 cm E horizon stored 12 ± 4 % of the total pyrogenic organic C. No increase in C stocks and no pyrogenic organic materials were observed in 60–100 cm in CoBC soils. We provide evidence of the downwards migration of a fraction of pyrogenic OM but limited to 60 cm 200 years after surface incorporation in this type of fine-textured soil such as the studied Luvisols. While 75 % of the difference in C stocks between CoBC and REF was made of pyrogenic organic C in the 0–30 cm Ap horizon, pyrogenic organic C only accounted for ~27 % of the C content difference in the 30–60 cm. Therefore, our study showed that the addition of a relatively small amount of pyrogenic OM could contribute to storing non-pyrogenic OM below 30 cm deep. As OM is more stabilized and persistent in subsoil than in topsoil, this storage of biochar-derived non-pyrogenic OM is likely persistent.

In 30–60 cm, the biochar accumulation led to a shift in the fraction contributing the most to the total C stock. In CoBC soils, most of the C occurred as free and occluded POM while most of the C was contained in the MAOM fraction in REF soils. In 30–60 cm, pyrogenic organic C was recovered in all size and density fractions. Although most of the pyrogenic organic C was recovered in free and occluded POM, ~25 % of the total pyrogenic organic C in the E horizon occurred as associated with mineral phases. Our study showed that most of the pyrogenic organic C has migrated downwards as POM, and mostly as sand-size POM. This suggests that particle leaching in macroporosity and bioturbation are likely major processes involved in the vertical transfers of biochar.

Soil pore water collected from suction cups during the winter wheat growing season revealed lower DOC concentrations and a greater bulk aromaticity of DOM in CoBC than in REF soils. Although biochar favors non-pyrogenic DOM adsorption, it is continuously dissolved and leached from surface layers ~200 years after accumulation. We can hypothesize that biochar aging, through its functionalization and decrease in hydrophobicity, promotes its solubility and transfer as dissolved pyrogenic organic C.

The DSC analysis on MAOM fractions corroborated the optical properties of DOM from CoBC soils. The continuous leaching of dissolved pyrogenic C and the presence of pyrogenic C onto MAOM fractions suggests that, in addition to its transport as particles, biochar could be continuously dissolved and leached from topsoil layers and adsorbed onto reactive minerals in the subsoils.

Overall, we clearly highlighted that surface amendments of biochar increased C stocks in both topsoil and subsoil horizons through both pyrogenic and non-pyrogenic OM storage. Therefore, it would be interesting to investigate the processes (e.g., stabilization, solubilization, microbial activity) promoting non-pyrogenic organic C contribution to biochar-driven C storage and their evolution with biochar aging. Furthermore, as we showed that century-old biochar is still solubilized, we believe further research studying the role of biochar as a hotspot of biogeochemical processes and investigated biochar solubilization and sorption onto soil minerals in subsoil would provide great insights in long term pyrogenic OM dynamics. Investigating the impact of biochar on the persistence of both pyrogenic and non-pyrogenic OM in the different soil fractions would also give useful information on the relevance of biochar amendment as a practice for C storage over the long term.

Declaration of Competing Interest

The authors declare that they have no known competing financial interests or personal relationships that could have appeared to influence the work reported in this paper.

Data availability

Data will be made available on request.

Acknowledgements

We would like to thank colleagues from the water-soil-plant exchange lab for their advice during the set-up of the field work and in particular Thomas Rochereau for his precious work in the lab. A special thanks goes to Alexandre Godfrind owner and farmer of the experimental site for his help in the field. We warmly thank the two anonymous reviewers for their supportive contributions and constructive comments which improved the quality of the manuscript. This research was funded through the Concerted Research Action grant 17/21-03 within the CHAR project framework by the French Community of Belgium.

Appendix A. Supplementary data

Supplementary data to this article can be found online at https://doi.org/10.1016/j.geoderma.2023.116717.

References

Abiven, S., Hengartner, P., Schneider, M.P.W., Singh, N., Schmidt, M.W.I., 2011. Pyrogenic carbon soluble fraction is larger and more aromatic in aged charcoal than in fresh charcoal. Soil Biol. Biochem. 43, 1615–1617. https://doi.org/10.1016/j.soilbio.2011.03.027.

Aller, D., Rathke, S., Laird, D., Cruse, R., Hatfield, J., 2017. Impacts of fresh and aged biochars on plant available water and water use efficiency. Geoderma 307, 114–121. https://doi.org/10.1016/j.geoderma.2017.08.007.

Angst, G., Mueller, K.E., Nierop, K.G.J., Simpson, M.J., 2021. Plant- or microbial-derived? A review on the molecular composition of stabilized soil organic matter. Soil Biol. Biochem. 156, 108189 https://doi.org/10.1016/j.soilbio.2021.108189.

Balesdent, J., Basile-Doelsch, I., Chadoeuf, J., Cornu, S., Derrien, D., Fekiacova, Z., Hatté, C., 2018. Atmosphere–soil carbon transfer as a function of soil depth. Nature 1. https://doi.org/10.1038/s41586-018-0328-3.

Batjes, N.h., 1996. Total carbon and nitrogen in the soils of the world. Eur. J. Soil Sci. 47, 151–163. https://doi.org/10.1111/j.1365-2389.1996.tb01386.x.

Begill, N., Don, A., Poeplau, C., 2023. No detectable upper limit of mineral-associated organic carbon in temperate agricultural soils. Glob. Chang. Biol. 29, 4662–4669. https://doi.org/10.1111/gcb.16804.

Biederman, L.A., Harpole, W.S., 2013. Biochar and its effects on plant productivity and nutrient cycling: a meta-analysis. GCB Bioenergy 5, 202–214. https://doi.org/10.1111/gcbb.12037.

Bird, M.I., Wynn, J.G., Saiz, G., Wurster, C.M., McBeath, A., 2015. The pyrogenic carbon cycle. Annu. Rev. Earth Planet. Sci. 43, 273–298. https://doi.org/10.1146/annurev-earth-060614-105038.

Birdwell, J.E., Engel, A.S., 2010. Characterization of dissolved organic matter in cave and spring waters using UV–Vis absorbance and fluorescence spectroscopy. Org Geochem. 41, 270–280. https://doi.org/10.1016/j.orggeochem.2009.11.002.

Bonhage, A., Raab, T., Schneider, A., Fischer, T., Ramezany, S., Ouimet, W., Raab, A., Hirsch, F., 2022. Vertical SOC distribution and aromatic carbon in centuries old charcoal-rich Technosols. Eur. J. Soil Sci. 73, e13293.

Borchard, N., Ladd, B., Eschemann, S., Hegenberg, D., Möseler, B.M., Amelung, W., 2014. Black carbon and soil properties at historical charcoal production sites in Germany. Geoderma 232–234, 236–242. https://doi.org/10.1016/j.geoderma.2014.05.007.

Bowring, S.P.K., Jones, M.W., Ciais, P., Guenet, B., Abiven, S., 2022. Pyrogenic carbon decomposition critical to resolving fire's role in the Earth system. Nat. Geosci. 15, 135–142. https://doi.org/10.1038/s41561-021-00892-0.

Brodowski, S., Amelung, W., Haumaier, L., Abetz, C., Zech, W., 2005. Morphological and chemical properties of black carbon in physical soil fractions as revealed by scanning electron microscopy and energy-dispersive X-ray spectroscopy. Geoderma 128, 116–129. https://doi.org/10.1016/j.geoderma.2004.12.019.

Burgeon, V., Fouché, J., Leifeld, J., Chenu, C., Cornélis, J.-T., 2021. Organo-mineral associations largely contribute to the stabilization of century-old pyrogenic organic matter in cropland soils. Geoderma 388, 114841. https://doi.org/10.1016/j.geoderma.2020.114841.

Burgeon, V., Fouché, J., Garré, S., Dehkordi, R.H., Colinet, G., Cornelis, J.-T., 2022. Young and century-old biochars strongly affect nutrient cycling in a temperate agroecosystem. Agr. Ecosyst. Environ. 328, 107847 https://doi.org/10.1016/j.agee.2021.107847.

Button, E.S., Pett-Ridge, J., Murphy, D.V., Kuzyakov, Y., Chadwick, D.R., Jones, D.L., 2022. Deep-C storage: biological, chemical and physical strategies to enhance carbon stocks in agricultural subsoils. Soil Biol. Biochem. 170, 108697 https://doi.org/10.1016/j.soilbio.2022.108697.

Carcaillet, C., 2001. Soil particles reworking evidences by AMS 14C dating of charcoal. C. R. Acad. Sci., Ser. IIA: Sci. - Earth Planet. Sci. 332, 21–28. https://doi.org/10.1016/S1251-8050(00)01485-3.

Cheng, C.-H., Lehmann, J., 2009. Ageing of black carbon along a temperature gradient. Chemosphere 75, 1021–1027. https://doi.org/10.1016/j.chemosphere.2009.01.045.

Cheng, C.-H., Lehmann, J., Thies, J.E., Burton, S.D., Engelhard, M.H., 2006. Oxidation of black carbon by biotic and abiotic processes. Org Geochem. 37, 1477–1488. https://doi.org/10.1016/j.orggeochem.2006.06.022.
Cheng, C.-H., Lehmann, J., Engelhard, M.H., 2008. Natural oxidation of black carbon in soils: Changes in molecular form and surface charge along a climosequence. Geochim. Cosmochim. Acta 72, 1598–1610. https://doi.org/10.1016/j.gca.2008.01.010.
Chenu, C., Angers, D.A., Barré, P., Derrien, D., Arrouays, D., Balesdent, J., 2019. Increasing organic stocks in agricultural soils: Knowledge gaps and potential innovations. Soil Tillage Res. 188, 41–52. https://doi.org/10.1016/j.still.2018.04.011.
Cooper, J., Greenberg, I., Ludwig, B., Hippich, L., Fischer, D., Glaser, B., Kaiser, M., 2020. Effect of biochar and compost on soil properties and organic matter in aggregate size fractions under field conditions. Agr. Ecosyst. Environ. 295, 106882 https://doi.org/10.1016/j.agee.2020.106882.
Cotrufo, M.F., Ranalli, M.G., Haddix, M.L., Six, J., Lugato, E., 2019. Soil carbon storage informed by particulate and mineral-associated organic matter. Nat. Geosci. 12, 989–994. https://doi.org/10.1038/s41561-019-0484-6.
Crane-Droesch, A., Abiven, S., Jeffery, S., Torn, M.S., 2013. Heterogeneous global crop yield response to biochar: a meta-regression analysis. Environ. Res. Lett. 8, 044049 https://doi.org/10.1088/1748-9326/8/4/044049.
Czimczik, C.I., Masiello, C.A., 2007. Controls on black carbon storage in soils. Global Biogeochem. Cycles 21. https://doi.org/10.1029/2006GB002798.
Dell'Abate, M.T., Benedetti, A., Sequi, P., 2000. Thermal methods of organic matter maturation monitoring during a composting process. J. Therm. Anal. Calorim. 61, 389–396. https://doi.org/10.1023/A:1010157115211.
Derrien, D., Barré, P., Basile-Doelsch, I., Cécillon, L., Chabbi, A., Crème, A., Fontaine, S., Henneron, L., Janot, N., Lashermes, G., Quénéa, K., Rees, F., Dignac, M.-F., 2023. Current controversies on mechanisms controlling soil carbon storage: implications for interactions with practitioners and policy-makers. A review. Agron. Sustain. Dev. 43, 21. https://doi.org/10.1007/s13593-023-00876-x.
Dittmar, T., de Rezende, C.E., Manecki, M., Niggemann, J., Coelho Ovalle, A.R., Stubbins, A., Bernardes, M.C., 2012. Continuous flux of dissolved black carbon from a vanished tropical forest biome. Nat. Geosci. 5, 618–622. https://doi.org/10.1038/ngeo1541.
Dove, N.C., Arogyaswamy, K., Billings, S.A., Botthoff, J.K., Carey, C.J., Cisco, C., DeForest, J.L., Fairbanks, D., Fierer, N., Gallery, R.E., Kaye, J.P., Lohse, K.A., Maltz, M.R., Mayorga, E., Pett-Ridge, J., Yang, W.H., Hart, S.C., Aronson, E.L., 2020. Continental-scale patterns of extracellular enzyme activity in the subsoil: an overlooked reservoir of microbial activity. Environ. Res. Lett. 15, 1040a1. https://doi.org/10.1088/1748-9326/abb0b3.
Eckmeier, E., Gerlach, R., Skjemstad, J.O., Ehrmann, O., Schmidt, M.W.I., 2007. Minor changes in soil organic carbon and charcoal concentrations detected in a temperate deciduous forest a year after an experimental slash-and-burn. Biogeosciences 4, 377–383. https://doi.org/10.5194/bg-4-377-2007.
Eusterhues, K., Rumpel, C., Kögel-Knabner, I., 2007. Composition and radiocarbon age of HF-resistant soil organic matter in a Podzol and a Cambisol. Org. Geochem. 38, 1356–1372. https://doi.org/10.1016/j.orggeochem.2007.04.001.
Eykelbosh, A.J., Johnson, M.S., Couto, E.G., 2015. Biochar decreases dissolved organic carbon but not nitrate leaching in relation to vinasse application in a Brazilian sugarcane soil. J. Environ. Manage. 149, 9–16. https://doi.org/10.1016/j.jenvman.2014.09.033.
Fellman, J.B., Hood, E., Spencer, R.G., 2010. Fluorescence spectroscopy opens new windows into dissolved organic matter dynamics in freshwater ecosystems: a review. Limnol. Oceanogr. 55, 2452–2462.
Fontaine, S., Barot, S., Barré, P., Bdioui, N., Mary, B., Rumpel, C., 2007. Stability of organic carbon in deep soil layers controlled by fresh carbon supply. Nature 450, 277–280. https://doi.org/10.1038/nature06275.
Forbes, M.S., Raison, R.J., Skjemstad, J.O., 2006. Formation, transformation and transport of black carbon (charcoal) in terrestrial and aquatic ecosystems. Sci. Total Environ. 370, 190–206. https://doi.org/10.1016/j.scitotenv.2006.06.007.
Fouché, J., Christiansen, C.T., Lafrenière, M.J., Grogan, P., Lamoureux, S.F., 2020. Canadian permafrost stores large pools of ammonium and optically distinct dissolved organic matter. Nat. Commun. 11, 1–11. https://doi.org/10.1038/s41467-020-18331-w.
Georgiou, K., Jackson, R.B., Vindušková, O., Abramoff, R.Z., Ahlström, A., Feng, W., Harden, J.W., Pellegrini, A.F.A., Polley, H.W., Soong, J.L., Riley, W.J., Torn, M.S., 2022. Global stocks and capacity of mineral-associated soil organic carbon. Nat. Commun. 13, 3797. https://doi.org/10.1038/s41467-022-31540-9.
Goidts, E., van Wesemael, B., 2007. Regional assessment of soil organic carbon changes under agriculture in Southern Belgium (1955–2005). Geoderma 141, 341–354. https://doi.org/10.1016/j.geoderma.2007.06.013.
Hardy, B., Cornelis, J.-T., Houben, D., Leifeld, J., Lambert, R., Dufey, J.E., 2017a. Evaluation of the long-term effect of biochar on properties of temperate agricultural soil at pre-industrial charcoal kiln sites in Wallonia, Belgium. Eur. J. Soil Sci. 68, 80–89. https://doi.org/10.1111/ejss.12395.
Hardy, B., Borchard, N., Leifeld, J., 2022. Identification of thermal signature and quantification of charcoal in soil using differential scanning calorimetry and benzene polycarboxylic acid (BPCA) markers. Soil 8, 451–466. https://doi.org/10.5194/soil-8-451-2022.
Hardy, B., Dufey, J.E., 2017. The resistance of centennial soil charcoal to the "Walkley-Black" oxidation. Geoderma 303, 37–43. https://doi.org/10.1016/j.geoderma.2017.05.001.
Hardy, B., Leifeld, J., Knicker, H., Dufey, J.E., Deforce, K., Cornélis, J.-T., 2017b. Long term change in chemical properties of preindustrial charcoal particles aged in forest and agricultural temperate soil. Org. Geochem. 107, 33–45. https://doi.org/10.1016/j.orggeochem.2017.02.008.
Heidarian Dehkordi, R., Burgeon, V., Fouché, J., Placencia Gomez, E., Cornelis, J.-T., Nguyen, F., Denis, A., Meersmans, J., 2020a. Using UAV collected RGB and multispectral images to evaluate winter wheat performance across a site characterized by century-old biochar patches in Belgium. Remote Sens. 12, 2504. https://doi.org/10.3390/rs12152504.
Heidarian Dehkordi, R., Denis, A., Fouché, J., Burgeon, V., Cornelis, J.T., Tychon, B., Placencia Gomez, E., Meersmans, J., 2020b. Remotely-sensed assessment of the impact of century-old biochar on chicory crop growth using high-resolution UAV-based imagery. Int. J. Appl. Earth Obs. Geoinf. 91, 102147 https://doi.org/10.1016/j.jag.2020.102147.
Heitkötter, J., Marschner, B., 2018. Soil zymography as a powerful tool for exploring hotspots and substrate limitation in undisturbed subsoil. Soil Biol. Biochem. 124, 210–217. https://doi.org/10.1016/j.soilbio.2018.06.021.
Hicks Pries, C., Ryals, R., Zhu, B., Min, K., Cooper, A., Goldsmith, S., Pett-Ridge, J., Torn, M., Asefaw Berhe, A., 2023. The deep soil organic carbon response to global change. Annu. Rev. Ecol. Evol. Syst. 54, null. https://doi.org/10.1146/annurev-ecolsys-102320-085332.
Hirsch, F., Raab, T., Ouimet, W., Dethier, D., Schneider, A., Raab, A., 2017. Soils on historic charcoal hearths: terminology and chemical properties. Soil Sci. Soc. Am. J. 81, 1427–1435. https://doi.org/10.2136/sssaj2017.02.0067.
Hobley, E., 2019. Vertical distribution of soil pyrogenic matter: a review. Pedosphere 29, 137–149. https://doi.org/10.1016/S1002-0160(19)60795-2.
Hockaday, W.C., Grannas, A.M., Kim, S., Hatcher, P.G., 2007. The transformation and mobility of charcoal in a fire-impacted watershed. Geochim. Cosmochim. Acta 71, 3432–3445. https://doi.org/10.1016/j.gca.2007.02.023.
IPCC, Shukla, P.R., Skea, J., Calvo Buendia, E., Masson-Delmotte, V., Pörtner, H.-O., Roberts, D.C., Zhai, P., Slade, P., Connors, S., van Diemen, R., Ferrat, M., Haughey, E., Luz, S., Neogi, S., Pathak, M., Petzold, J., Portugal Pereira, J., Vyas, P., Huntley, E., Kissick, K., Belkacemi, M., Malley, J., 2019. Climate Change and Land: an IPCC special report on climate change, desertification, land degradation, sustainable land management, food security, and greenhouse gas fluxes in terrestrial ecosystems. IPCC.
IUSS Working Group WRB, 2015. World Reference Base for Soil Resources 2014, update 2015 International soil classification system for naming soils and creating legends for soil maps. World Soil Resources Reports No. 106. FAO, Rome.
Jamieson, T., Sager, E., Guéguen, C., 2014. Characterization of biochar-derived dissolved organic matter using UV–visible absorption and excitation–emission fluorescence spectroscopies. Chemosphere 103, 197–204. https://doi.org/10.1016/j.chemosphere.2013.11.066.
Jeffery, S., Verheijen, F.G.A., van der Velde, M., Bastos, A.C., 2011. A quantitative review of the effects of biochar application to soils on crop productivity using meta-analysis. Agr. Ecosyst. Environ. 144, 175–187. https://doi.org/10.1016/j.agee.2011.08.015.
Jiang, S., Nguyen, T.A.H., Rudolph, V., Yang, H., Zhang, D., Ok, Y.S., Huang, L., 2017. Characterization of hard- and softwood biochars pyrolyzed at high temperature. Environ. Geochem. Health 39, 403–415. https://doi.org/10.1007/s10653-016-9873-6.
Jobbágy, E.G., Jackson, R.B., 2000. The vertical distribution of soil organic carbon and its relation to climate and vegetation. Ecol. Appl. 10, 423–436. https://doi.org/10.1890/1051-0761(2000)010[0423:TVDOSO]2.0.CO;2.
Joseph, S., Cowie, A.L., Van Zwieten, L., Bolan, N., Budai, A., Buss, W., Cayuela, M.L., Graber, E.R., Ippolito, J.A., Kuzyakov, Y., Luo, Y., Ok, Y.S., Palansooriya, K.N., Shepherd, J., Stephens, S., Weng, Z.(Han), Lehmann, J., 2021. How biochar works, and when it doesn't: A review of mechanisms controlling soil and plant responses to biochar. GCB Bioenergy 13, 1731–1764. https://doi.org/10.1111/gcbb.12885.
Kaiser, K., Kalbitz, K., 2012. Cycling downwards – dissolved organic matter in soils. Soil Biol. Biochem. 52, 29–32. https://doi.org/10.1016/j.soilbio.2012.04.002.
Kerré, B., Bravo, C.T., Leifeld, J., Cornelissen, G., Smolders, E., 2016. Historical soil amendment with charcoal increases sequestration of non-charcoal carbon: a comparison among methods of black carbon quantification. Eur. J. Soil Sci. 67, 324–331. https://doi.org/10.1111/ejss.12338.
Kerré, B., Willaert, B., Smolders, E., 2017. Lower residue decomposition in historically charcoal-enriched soils is related to increased adsorption of organic matter. Soil Biol. Biochem. 104, 1–7. https://doi.org/10.1016/j.soilbio.2016.10.007.
Kleber, M., Sollins, P., Sutton, R., 2007. A conceptual model of organo-mineral interactions in soils: self-assembly of organic molecular fragments into zonal structures on mineral surfaces. Biogeochemistry 85, 9–24.
Knicker, H., 2011. Pyrogenic organic matter in soil: Its origin and occurrence, its chemistry and survival in soil environments. Q. Int. 243, 251–263. https://doi.org/10.1016/j.quaint.2011.02.037.
Kögel-Knabner, I., Guggenberger, G., Kleber, M., Kandeler, E., Kalbitz, K., Scheu, S., Eusterhues, K., Leinweber, P., 2008. Organo-mineral associations in temperate soils: integrating biology, mineralogy, and organic matter chemistry. J. Plant Nutr. Soil Sci. 171, 61–82. https://doi.org/10.1002/jpln.200700048.
Kuzyakov, Y., Bogomolova, I., Glaser, B., 2014. Biochar stability in soil: decomposition during eight years and transformation as assessed by compound-specific 14C analysis. Soil Biol. Biochem. 70, 229–236. https://doi.org/10.1016/j.soilbio.2013.12.021.
Lavallee, J.M., Soong, J.L., Cotrufo, M.F., 2020. Conceptualizing soil organic matter into particulate and mineral-associated forms to address global change in the 21st century. Glob. Chang. Biol. 26, 261–273. https://doi.org/10.1111/gcb.14859.
Lawaetz, A.J., Stedmon, C.A., 2009. Fluorescence intensity calibration using the Raman scatter peak of water. Appl. Spectrosc. 63, 936–940.
Lehmann, J., 2007a. A handful of carbon. Nature 447, 143–144. https://doi.org/10.1038/447143a.

Lehmann, J., 2007b. Bio-energy in the black. Front. Ecol. Environ. 5, 381–387. https://doi.org/10.1890/1540-9295(2007)5[381:BITB]2.0.CO;2.
Leifeld, J., 2007. Thermal stability of black carbon characterised by oxidative differential scanning calorimetry. Org Geochem. 38, 112–127. https://doi.org/10.1016/j.orggeochem.2006.08.004.
Liu, C., Wang, H., Li, P., Xian, Q., Tang, X., 2019. Biochar's impact on dissolved organic matter (DOM) export from a cropland soil during natural rainfalls. Sci. Total Environ. 650, 1988–1995. https://doi.org/10.1016/j.scitotenv.2018.09.356.
Lopez-Capel, E., Sohi, S.P., Gaunt, J.L., Manning, D.A.C., 2005. Use of thermogravimetry-differential scanning calorimetry to characterize modelable soil organic matter fractions. Soil Sci. Soc. Am. J. 69, 136–140. https://doi.org/10.2136/sssaj2005.0136a.
Lugato, E., Lavallee, J.M., Haddix, M.L., Panagos, P., Cotrufo, M.F., 2021. Different climate sensitivity of particulate and mineral-associated soil organic matter. Nat. Geosci. 14, 295–300. https://doi.org/10.1038/s41561-021-00744-x.
Luo, Z., Wang, G., Wang, E., 2019. Global subsoil organic carbon turnover times dominantly controlled by soil properties rather than climate. Nat. Commun. 10, 3688. https://doi.org/10.1038/s41467-019-11597-9.
Lutfalla, S., Abiven, S., Barré, P., Wiedemeier, D.B., Christensen, B.T., Houot, S., Kätterer, T., Macdonald, A.J., van Oort, F., Chenu, C., 2017. Pyrogenic Carbon Lacks Long-Term Persistence in Temperate Arable Soils. Front. Earth Sci. 5.
Major, J., Lehmann, J., Rondon, M., Goodale, C., 2010. Fate of soil-applied black carbon: downward migration, leaching and soil respiration. Glob. Chang. Biol. 16, 1366–1379. https://doi.org/10.1111/j.1365-2486.2009.02044.x.
Mastrolonardo, G., Calderaro, C., Cocozza, C., Hardy, B., Dufey, J., Cornelis, J.-T., 2019. Long-term effect of charcoal accumulation in hearth soils on tree growth and nutrient cycling. Front. Environ. Sci. 7.
McKnight, D.M., Boyer, E.W., Westerhoff, P.K., Doran, P.T., Kulbe, T., Andersen, D.T., 2001. Spectrofluorometric characterization of dissolved organic matter for indication of precursor organic material and aromaticity. Limnol. Oceanogr. 46, 38–48.
Meersmans, J., van Wesemael, B., De Ridder, F., Van Molle, M., 2009. Modelling the three-dimensional spatial distribution of soil organic carbon (SOC) at the regional scale (Flanders, Belgium). Geoderma 152, 43–52. https://doi.org/10.1016/j.geoderma.2009.05.015.
Murphy, K.R., Stedmon, C.A., Waite, T.D., Ruiz, G.M., 2008. Distinguishing between terrestrial and autochthonous organic matter sources in marine environments using fluorescence spectroscopy. Mar. Chem. 108, 40–58. https://doi.org/10.1016/j.marchem.2007.10.003.
Murphy, K., Stedmon, C., Graeber, D., Bro, R., 2013. Fluorescence spectroscopy and multi-way techniques. PARAFAC. Anal. Methods 5, 6557–6566. https://doi.org/10.1039/C3AY41160E.
Murphy, K.R., Stedmon, C.A., Wenig, P., Bro, R., 2014. OpenFluor- an online spectral library of auto-fluorescence by organic compounds in the environment. Anal. Methods 6, 658–661. https://doi.org/10.1039/C3AY41935E.
Nachimuthu, G., Watkins, M.D., Hulugalle, N., Finlay, L.A., 2020. Storage and initial processing of water samples for organic carbon analysis in runoff. MethodsX 7, 101012. https://doi.org/10.1016/j.mex.2020.101012.
Paustian, K., Lehmann, J., Ogle, S., Reay, D., Robertson, G.P., Smith, P., 2016. Climate-smart soils. Nature 532, 49–57. https://doi.org/10.1038/nature17174.
Plante, A.F., Fernández, J.M., Leifeld, J., 2009. Application of thermal analysis techniques in soil science. Geoderma 153, 1–10. https://doi.org/10.1016/j.geoderma.2009.08.016.
Poeplau, C., Don, A., Six, J., Kaiser, M., Benbi, D., Chenu, C., Cotrufo, M.F., Derrien, D., Gioacchini, P., Grand, S., Gregorich, E., Griepentrog, M., Gunina, A., Haddix, M., Kuzyakov, Y., Kühnel, A., Macdonald, L.M., Soong, J., Trigalet, S., Vermeire, M.-L., Rovira, P., van Wesemael, B., Wiesmeier, M., Yeasmin, S., Yevdokimov, I., Nieder, R., 2018. Isolating organic carbon fractions with varying turnover rates in temperate agricultural soils – A comprehensive method comparison. Soil Biol. Biochem. 125, 10–26. https://doi.org/10.1016/j.soilbio.2018.06.025.
Poirier, V., Roumet, C., Munson, A.D., 2018. The root of the matter: Linking root traits and soil organic matter stabilization processes. Soil Biol. Biochem. 120, 246–259. https://doi.org/10.1016/j.soilbio.2018.02.016.
Pucher, M., Wünsch, U., Weigelhofer, G., Murphy, K., Hein, T., Graeber, D., 2019. staRdom: Versatile software for analyzing spectroscopic data of dissolved organic matter in R. Water 11, 2366. https://doi.org/10.3390/w11112366.
R Core Team, 2022. R: A Language and Environment for Statistical Computing.
Rasse, D.P., Rumpel, C., Dignac, M.-F., 2005. Is soil carbon mostly root carbon? Mechanisms for a specific stabilisation. Plant Soil 269, 341–356. https://doi.org/10.1007/s11104-004-0907-y.
Reisser, M., Purves, R.S., Schmidt, M.W.I., Abiven, S., 2016. Pyrogenic carbon in soils: a literature-based inventory and a global estimation of its content in soil organic carbon and stocks. Front. Earth Sci. 4, 80. https://doi.org/10.3389/feart.2016.00080.
Rocci, K.S., Lavallee, J.M., Stewart, C.E., Cotrufo, M.F., 2021. Soil organic carbon response to global environmental change depends on its distribution between mineral-associated and particulate organic matter: A meta-analysis. Sci. Total Environ. 793, 148569 https://doi.org/10.1016/j.scitotenv.2021.148569.
Roth, V.-N., Lange, M., Simon, C., Hertkorn, N., Bucher, S., Goodall, T., Griffiths, R.I., Mellado-Vázquez, P.G., Mommer, L., Oram, N.J., Weigelt, A., Dittmar, T., Gleixner, G., 2019. Persistence of dissolved organic matter explained by molecular changes during its passage through soil. Nat. Geosci. 12, 755–761. https://doi.org/10.1038/s41561-019-0417-4.
Rumpel, C., Kögel-Knabner, I., 2011. Deep soil organic matter—a key but poorly understood component of terrestrial C cycle. Plant and Soil 338, 143–158. https://doi.org/10.1007/s11104-010-0391-5.
Rumpel, C., Leifeld, J., Santin, C., Doerr, S.H., 2015. Movement of biochar in the environment. In: Biochar for Environmental Management, Routledge, pp. 283–299. https://doi.org/10.4324/9780203762264-11.
Salomé, C., Nunan, N., Pouteau, V., Lerch, T.Z., Chenu, C., 2010. Carbon dynamics in topsoil and in subsoil may be controlled by different regulatory mechanisms. Glob. Chang. Biol. 16, 416–426. https://doi.org/10.1111/j.1365-2486.2009.01884.x.
Schiedung, M., Bellè, S.-L., Sigmund, G., Kalbitz, K., Abiven, S., 2020. Vertical mobility of pyrogenic organic matter in soils: a column experiment. Biogeosciences 17, 6457–6474. https://doi.org/10.5194/bg-17-6457-2020.
Schmidt, M.W.I., Noack, A.G., 2000. Black carbon in soils and sediments: analysis, distribution, implications, and current challenges. Global Biogeochem. Cycles 14, 777–793. https://doi.org/10.1029/1999GB001208.
Schmidt, M.W.I., Torn, M.S., Abiven, S., Dittmar, T., Guggenberger, G., Janssens, I.A., Kleber, M., Kogel-Knabner, I., Lehmann, J., Manning, D.A.C., Nannipieri, P., Rasse, D.P., Weiner, S., Trumbore, S.E., 2011. Persistence of soil organic matter as an ecosystem property. Nature 478, 49–56.
Six, J., Elliott, E.t., Paustian, K., Doran, J.W., 1998. Aggregation and soil organic matter accumulation in cultivated and native grassland soils. Soil Sci. Soc. Am. J. 62, 1367–1377. https://doi.org/10.2136/sssaj1998.03615995006200050032x.
Smebye, A., Alling, V., Vogt, R.D., Gadmar, T.C., Mulder, J., Cornelissen, G., Hale, S.E., 2016. Biochar amendment to soil changes dissolved organic matter content and composition. Chemosphere 142, 100–105. https://doi.org/10.1016/j.chemosphere.2015.04.087.
Smith, P., 2016. Soil carbon sequestration and biochar as negative emission technologies. Glob. Chang. Biol. 22, 1315–1324. https://doi.org/10.1111/gcb.13178.
Sokol, N.W., Sanderman, J., Bradford, M.A., 2018. Pathways of mineral-associated soil organic matter formation: integrating the role of plant carbon source, chemistry, and point of entry. Glob. Chang. Biol. https://doi.org/10.1111/gcb.14482.
Soucémarianadin, L., Reisser, M., Cécillon, L., Barré, P., Nicolas, M., Abiven, S., 2019. Pyrogenic carbon content and dynamics in top and subsoil of French forests. Soil Biol. Biochem. 133, 12–15. https://doi.org/10.1016/j.soilbio.2019.02.013.
Spokas, K.A., Novak, J.M., Masiello, C.A., Johnson, M.G., Colosky, E.C., Ippolito, J.A., Trigo, C., 2014. Physical disintegration of biochar: an overlooked process. Environ. Sci. Technol. Lett. 1, 326–332. https://doi.org/10.1021/ez500199t.
Stedmon, C.A., Bro, R., 2008. Characterizing dissolved organic matter fluorescence with parallel factor analysis: a tutorial. Limnol. Oceanogr. Methods 6, 572–579. https://doi.org/10.4319/lom.2008.6.572b.
Stewart, C.E., Paustian, K., Conant, R.T., Plante, A.F., Six, J., 2007. Soil carbon saturation: concept, evidence and evaluation. Biogeochemistry 86, 19–31. https://doi.org/10.1007/s10533-007-9140-0.
Tang, J., Li, X., Luo, Y., Li, G., Khan, S., 2016. Spectroscopic characterization of dissolved organic matter derived from different biochars and their polycylic aromatic hydrocarbons (PAHs) binding affinity. Chemosphere 152, 399–406. https://doi.org/10.1016/j.chemosphere.2016.03.016.
Vidal, A., Watteau, F., Remusat, L., Mueller, C.W., Nguyen Tu, T.-T., Buegger, F., Derenne, S., Quenea, K., 2019. Earthworm cast formation and development: a shift from plant litter to mineral associated organic matter. Front. Environ. Sci. 7, 55. https://doi.org/10.3389/fenvs.2019.00055.
Virto, I., Moni, C., Swanston, C., Chenu, C., 2010. Turnover of intra- and extra-aggregate organic matter at the silt-size scale. Geoderma 156, 1–10. https://doi.org/10.1016/j.geoderma.2009.12.028.
von Lützow, M., Kögel-Knabner, I., Ekschmitt, K., Flessa, H., Guggenberger, G., Matzner, E., Marschner, B., 2007. SOM fractionation methods: Relevance to functional pools and to stabilization mechanisms. Soil Biol. Biochem. 39, 2183–2207. https://doi.org/10.1016/j.soilbio.2007.03.007.
Wagner, S., Jaffé, R., Stubbins, A., 2018. Dissolved black carbon in aquatic ecosystems. Limnol. Oceanogr. Lett. 3, 168–185. https://doi.org/10.1002/lol2.10076.
Walkley, A., Black, I.A., 1934. An examination of the Degtjareff method for determining soil organic matter, and a proposed modification of the chromic acid titration method. Soil Sci. 37, 29.
Weishaar, J.L., Aiken, G.R., Bergamaschi, B.A., Fram, M.S., Fujii, R., Mopper, K., 2003. Evaluation of specific ultraviolet absorbance as an indicator of the chemical composition and reactivity of dissolved organic carbon. Environ. Sci. Tech. 37, 4702–4708. https://doi.org/10.1021/es030360x.
Whalen, E.D., Grandy, A.S., Sokol, N.W., Keiluweit, M., Ernakovich, J., Smith, R.G., Frey, S.D., 2022. Clarifying the evidence for microbial- and plant-derived soil organic matter, and the path toward a more quantitative understanding. Glob. Chang. Biol. 28, 7167–7185. https://doi.org/10.1111/gcb.16413.
Wiedemeier, D.B., Abiven, S., Hockaday, W.C., Keiluweit, M., Kleber, M., Masiello, C.A., McBeath, A.V., Nico, P.S., Pyle, L.A., Schneider, M.P.W., Smernik, R.J., Wiesenberg, G.L.B., Schmidt, M.W.I., 2015. Aromaticity and degree of aromatic condensation of char. Org Geochem. 78, 135–143. https://doi.org/10.1016/j.orggeochem.2014.10.002.
Yang, Y., Sun, K., Han, L., Chen, Y., Liu, J., Xing, B., 2022. Biochar stability and impact on soil organic carbon mineralization depend on biochar processing, aging and soil clay content. Soil Biol. Biochem. 169, 108657 https://doi.org/10.1016/j.soilbio.2022.108657.